Analyzing Correlation Functions with Spherical and Cartesian Harmonics

Pawel Danielewicz
Department of Physics and Astronomy, and National Superconducting Cyclotron Laboratory
Michigan State University, East Lansing Michigan, 48824

Scott Pratt
Department of Physics and Astronomy
Michigan State University,
East Lansing Michigan, 48824
(Dated: May 19, 2006)

Correlation functions are typically expressed in terms of the three components of the relative momentum. In this paper, the benefits of using spherical or Cartesian harmonics to describe the angular information are presented. The physical content of specific angular projections is described and the resolving power of different classes of interactions is studied for correlations from symmetrization and from strong and Coulomb interactions. Gaussian sources and blast-wave examples are investigated in detail.

I. INTRODUCTION

Correlation measurements provide details of the size and shape of sources in heavy-ion reactions [1–4]. This information also permits the extraction of lifetime parameters of the emission which are closely linked to the equation of state. Perhaps the most major surprise for the first few years of results from the Relativistic Heavy Ion Collider (RHIC) is that experimentally determined source sizes [5–7] are in disagreement with predictions from hydrodynamic models which incorporate a phase transition [8–11]. The most studied correlations involve symmetrization effects of identical bosons, where the measured correlation, which is a function of the relative momentum, is linked to the source function, which is a function of the relative separation in coordinate space, by a simple Fourier transform. It is more difficult to extract source information resulting from other classes of correlation, such as those induced by strong or Coulomb interactions. This is especially true for information concerning the shape of the source. In this paper, we investigate the advantages of analyzing correlations and source functions as expansions of spherical harmonics. We find that this basis provides a convenient means for isolating and focusing on specific properties of the source. For instance, the $\ell = 2$ moments directly address the ratios of the varies dimensions of the source, e.g., $R_{\rm out}/R_{\rm side}$. Examples are provided to illustrate how different classes of interactions, such as strong or Coulomb, can be exploited to view different properties of the source.

The correlation from final-state interactions between two particles can be linked to the characteristics of the emission function through the relation,

$$1 + \mathcal{R}(\mathbf{P}, \mathbf{q}) = \int |\phi(\mathbf{q}, \mathbf{r})|^2 \mathcal{S}(\mathbf{P}, \mathbf{r}) d^3r. \tag{1}$$

Here, $\mathcal{R}(\mathbf{P}, \mathbf{q})$ is the difference of the correlation function from unity where $\mathbf{P}$ is the total momentum of the pair and $\mathbf{q}$ is the relative momentum measured in the two-particle rest frame. The distribution $\mathcal{S}(\mathbf{P}, \mathbf{r})$ describes the probability that two particles of types a and b with the same velocity $\mathbf{V}$ and with total momentum $\mathbf{P}$ are separated by $\mathbf{r}$, which can be determined by the single-particle emission probabilities $s_a(p, x)$.

$$\mathcal{S}(\mathbf{P}, \mathbf{r}') = \frac{\int d^4x_a d^4x_b s_a(m_a\mathbf{P}/(m_a+m_b), x_a) s_b(m_b\mathbf{P}/(m_a+m_b), x_b) \delta^3(\mathbf{r}' - \mathbf{r}'_a - \mathbf{r}'_b)}{\int d^4x_a d^4x_b s_a(m_a\mathbf{P}/(m_a+m_b), x_a) s_b(m_b\mathbf{P}/(m_a+m_b), x_b)}, \tag{2}$$

where $s_a(\mathbf{p}, x)$ is the probability of emitting a particle of momentum $\mathbf{p}$ from space-time point x, and $\mathbf{r}'_a$ is the position of the emission as measured by an observer moving with velocity $\mathbf{V}$. A detailed derivation of Eq. (1) can be found in [12]. Within the context of Eq. (1), one can at most determine the distribution of relative coordinates $\mathcal{S}(\mathbf{P}, \mathbf{r})$. Temporal information can only be inferred from the size and shape of the probability cloud described by $\mathcal{S}$ [13–15].

The principal challenge of correlation phenomenology is to extract all possible information concerning $\mathcal{S}(\mathbf{P}, \mathbf{r})$ from the measurement of $\mathcal{R}(\mathbf{P}, \mathbf{q})$. Since each value of $\mathbf{P}$ represents a different problem, we suppress the $\mathbf{P}$ labels which allows Eq. (1) to be expressed more simply,

$$\mathcal{R}(\mathbf{q}) = \int \left[|\phi(\mathbf{q}, \mathbf{r})|^2 - 1 \right] \mathcal{S}(\mathbf{r}) d^3r, \tag{3}$$

where it is hereafter assumed that $\mathbf{q}$ and $\mathbf{r}$ are evaluated in the center of mass frame where $\mathbf{P} = 0$. Determining $\mathcal{S}(\mathbf{r})$ can then be viewed as a matrix inversion problem where the different values of $\mathbf{q}$ represent vector indices of $\mathcal{R}$ and the values of $\mathbf{r}$ represent vector indices for the vector $\mathcal{S}$, while $|\phi^2(\mathbf{q},\mathbf{r})|^2 - 1$ then acts as a matrix. The process of performing this inversion is often referred to as "imaging" [16–21].

Imaging has been performed in detail for angle-averaged correlation functions, $\mathcal{R}(q)$, which can provide angle-averaged distributions $\mathcal{S}(r)$. It is the goal of this paper to describe how one might extract the angular information in $\mathcal{S}(\mathbf{r})$ by decomposing $\mathcal{R}(\mathbf{q})$ with spherical and Cartesian harmonics. Since $\phi(\mathbf{q},\mathbf{r})$ is a function of the magnitudes q and r and θ_{qr}, the relative angle between $\mathbf{q}$ and $\mathbf{r}$, $|\phi|^2$ is invariant to rotations. One can then use identities for spherical harmonics to show [19]

$$\mathcal{R}_{\ell,m}(q) = \int 4\pi r^2 dr\ \mathcal{K}_\ell(q,r)\ \mathcal{S}_{\ell,m}(r). \tag{4}$$

Here, expansions in terms of spherical harmonics are defined by the relations,

$$\begin{aligned} \mathcal{R}_{\ell,m}(q) &\equiv (4\pi)^{-1/2} \int d\Omega_q \mathcal{R}(\mathbf{q}) Y_{\ell,m}(\Omega), \\ \mathcal{R}(\mathbf{q}) &= (4\pi)^{1/2} \sum_{\ell,m} \mathcal{R}_{\ell,m}(q) Y_{\ell,m}(\Omega), \end{aligned} \tag{5}$$

with analogous expressions for the expansion of the source function. The kernel encodes the information from the wave function,

$$\mathcal{K}_\ell(q,r) \equiv \frac{1}{2} \int d\cos\theta_{qr} \left[|\phi(q,r,\cos\theta_{qr})|^2 - 1 \right] P_\ell(\cos\theta_{qr}). \tag{6}$$

The problem is thus reduced to a series of one-dimensional inversions for each (L,M) combination with a different matrix for each ℓ. Since Cartesian harmonics, $\mathcal{A}_{\vec{\ell}}(\Omega)$, of order $\ell = \ell_x + \ell_y + \ell_z$ are linear combinations of spherical harmonics of the same order, there are corresponding expressions to Eq. (4) and Eq. (5) with Cartesian harmonics,

$$\mathcal{R}_{\vec{\ell}}(q) = \int 4\pi r^2 dr\ \mathcal{K}_\ell(q,r)\ \mathcal{S}_{\vec{\ell}}(r), \tag{7}$$

where expansions of functions in terms of Cartesian harmonics are defined by

$$\begin{aligned} \mathcal{R}_{\vec{\ell}}(q) &\equiv \frac{(2\ell+1)!!}{\ell!} \int \frac{d\Omega_q}{4\pi} \mathcal{R}(\mathbf{q}) \mathcal{A}_{\vec{\ell}}(\Omega_q) \\ \mathcal{R}(\mathbf{q}) &= \sum_{\vec{\ell}} \frac{\ell!}{\ell_x!\ell_y!\ell_z!} \mathcal{R}_{\vec{\ell}} \hat{q}_x^{\ell_x} \hat{q}_y^{\ell_y} \hat{q}_z^{\ell_z}. \end{aligned} \tag{8}$$

In the next section, the structure of the kernel $\mathcal{K}_\ell$ is investigated for identical-particle interference and for strong and Coulomb interactions. We find that all three classes of interactions provide significant resolving power for all ℓ. Section III provides a detailed description of the properties of Cartesian harmonics. The subsequent section presents a discussion of the value of higher moments and shows how to relate specific angular projections to geometric properties of the source. In particular, we see that one can view the offset between the probability clouds for two different species with the $\ell = 1$ moments, the eccentricity and orientation of the elliptic properties of the source with the $\ell = 2$ moments, and the "boomerang" shape of source from the octupole ($\ell = 3$) moments. In Sec. V Gaussian and blast wave examples are evaluated in detail. In the final section, we summarize our results and discuss the prospects and challenges we expect to encounter in such analyses.

II. CORRELATION KERNELS, $\mathcal{K}_\ell(q,r)$

The ability of correlation functions to determine source characteristics depends on the correlation kernel $\mathcal{K}_\ell(q,r)$ which is defined in Eq.s (4) and (5). If one discretizes $\mathcal{K}_\ell(q,r)$ for specific values of q and r, the kernel can be thought of as a matrix. The matrix is real, and if it is not singular, can be inverted. One could then simple multiply the matrix $\mathcal{R}_{\ell,m}(q)$ by $\mathcal{K}_\ell^{-1}(q,r)$ and find $\mathcal{S}_\ell(q,r)$. Another tactic would be two parameterize the source function, then determine the parameters by fitting $\mathcal{R}_{\ell,m}(q)$. These tactics has been successfully pursued for the $\ell = 0$ case [16–21]. Evidence for non-Gaussian components in $\mathcal{S}_{L=0}(r)$ was found, especially for proton sources in intermediate energy

collisions. The procedure is not without difficulty as the answer could be quite sensitive to noise since errors in a given bin of q carry over to several different values of r and the stability of the answer can depend on the choice of the initial mesh.

In this section, we wish to demonstrate the resolving power of the kernel for different values of ℓ and for different classes of interactions. Kernels for the simple case of identical-boson interferometry are discussed in the first subsection, while the Coulomb and strong interactions are investigated in the subsequent subsections. It is crucial to understand the form and properties of the kernels before embarking on ambitious inversion procedures.

Since $\mathcal{S}(\mathbf{r})$ can be expanded in a Taylor series about $\mathbf{r} = 0$, $\mathcal{S}^{(\ell)}(r)$ always grows as r^L for small r. This means that, especially at large ℓ, the structure of the kernel for small r is not very important. Thus, we will be careful to study the form of the kernels at large r.

A. Kernels for Identical Bosons

For identical bosons, the squared relative wave function is

$$|\phi(q, r, \cos\theta_{qr})|^2 = 1 + \cos(2qr\cos\theta_{qr}), \tag{9}$$

where the convention for the relative momentum is that $\mathbf{q}$ refers to the momentum of one of the particles in the center-of-mass frame. The cosine term can be considered the real part of $e^{2i\mathbf{q}\cdot\mathbf{r}}$, which can be expanded in spherical Bessel functions.

$$\mathcal{K}_\ell(q, r) = \begin{cases} (i)^L j_\ell(2qr), & \text{even } L \\ 0, & \text{odd } L \end{cases} \tag{10}$$

Since $j_\ell(2qr) \sim (2qr)^L/L!!$ for small qr, one can see that there is little sensitivity to the structure of $\mathcal{S}_{L\neq 0}(q, r)$ at small r unless q is large. Thus, as is typical in Fourier transforms, information in $\mathcal{R}_\ell$ at large q is related to the structure of $\mathcal{S}_{\ell,m}$ at small r and vice versa. Furthermore, using the completeness relation,

$$\int_0^\infty j_\ell(2qr) j_\ell(2qr') q^2 dq = \frac{\pi}{16}\delta(r - r'), \tag{11}$$

it is straight-forward to find the inverse of $\mathcal{K}_\ell(q, r)$ from Eq. (4).

$$\mathcal{S}_{\ell,m}(r) = \int 4\pi q^2 dq\ \mathcal{R}_{\ell,m}(q)\mathcal{K}_\ell^{-1}(q, r), \tag{12}$$

$$\mathcal{K}_\ell^{-1}(q, r) = \frac{i^\ell}{\pi^3} j_\ell(2qr), \quad \text{even } \ell. \tag{13}$$

B. Kernels for the Coulomb Interaction

The Coulomb interaction also provides leverage for determining properties of $\mathcal{S}(\mathbf{r})$ from $\mathcal{R}(\mathbf{q})$ [22, 23]. Unfortunately, in this case inversion is not simple. Instead, one must carefully inspect the form of the kernel to understand the information contained in $\mathcal{R}(\mathbf{q})$. Unlike the kernel for identical particles, which depends solely on $qr/\hbar$ and $\cos\theta_{qr}$, the squared Coulomb wave function has an additional dependence on the parameter,

$$x = \frac{2\mu e^2}{q^2 r}, \tag{14}$$

where μ is the reduced mass, Here, x is the ratio of the potential and kinetic energy. The fact the $|\phi(\mathbf{q}, \mathbf{r})|^2$ depends on three parameters rather than two significantly complicates the relations between $\mathcal{R}$ and $\mathcal{S}$.

In the limit that qr is large (or $\hbar \to 0$), the wave function will then depend only on x and $\cos\theta_{qr}$. One can then find the equivalent classical expression for the squared wave function by calculating the density of states [22],

$$\begin{aligned} |\phi(q, r, \cos\theta_{qr})|^2 &\to \frac{d^3 q_0}{d^3 q} \\ &= \frac{1 + \cos\theta_{qr} - x}{\sqrt{(1 + \cos\theta_{qr} - x)^2 - x^2}} \Theta(1 + \cos\theta_{qr} - 2x), \end{aligned} \tag{15}$$

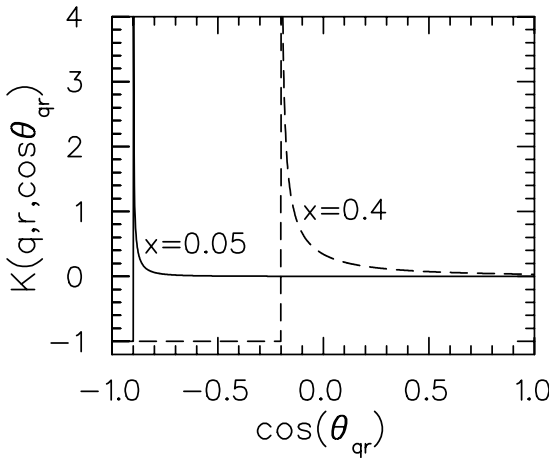

FIG. 1: The kernel, $K(q, r, \cos\theta_{qr}) = \phi^2 - 1$, for classical repulsive Coulomb forces are shown as a function of $\cos\theta_{qr}$. The structure for $\cos\theta_{qr} \sim -1$ is due to the deflection of the trajectories by the repulsive forces. The classical kernel depends only on $\cos\theta_{qr}$ and the dimensionless parameter, $x = 2\mu e^2/q^2 r$. For large momentum, or for large separations, the kernel is non-zero for a shrinking range of angles.

where $\mathbf{q_0}$ is the relative momentum when the particles were separated by $\mathbf{r}$. For small x the deviation of $|\phi|^2$ from unity is confined to a small region of angles near $\cos\theta_{qr} \sim -1$ as shown in Fig. 1 where the kernel is plotted for repelling charges. For these angles the trajectory must directly traverse the repelling charge and the kernel falls to -1 which means there is no path where the charges can emerge with that angle. The blocked trajectories pile up at slightly larger angles. The pile-up results in an integrable singularity in the kernel as shown by the peaks in Fig. 1. For small values of ℓ, the convolution with $P_\ell(\cos\theta_{qr})$ in Eq. (5) is insensitive to the small scale angular structure of the squared wave function and one can approximate the angular structure as a δ function.

$$|\phi(q, r, \cos\theta_{qr})|^2 \approx 1 - \frac{x}{2}\delta(1 - \cos\theta_{qr}),\ xL << 1. \tag{16}$$

Since $P_\ell(\cos\theta = -1) = (-1)^L$, the kernel can then be approximated as,

$$\mathcal{K}_\ell(q, r) \approx (-1)^L x/2,\ \text{for } |x| << 1, qr >> 1. \tag{17}$$

For characteristic radii of heavy ion collisions, ~ 5 fm, x does tend to be small for values of q much greater than 25 MeV/c. When q becomes smaller than 25 MeV/c, $qr/\hbar$ often falls below unity and quantum effects dominate. For more massive pairs x becomes larger and the approximation of Eq. (15) loses validity.

For small r quantum mechanics is important since particles can tunnel into the Coulomb or the angular momentum barrier. Unlike the classical expression, Coulomb wave functions are analytic near $r = 0$ and the squared wave function can be expanded in a Taylor expansion with powers $r^n(1-\cos\theta_{qr})^n$. Since the n^{th} term has no harmonic components with $\ell > n$, $\mathcal{K}_\ell$ must behave as r^L for $r \sim 0$. For a given r the lower limit q for which one could reach r without tunneling for a particle of momentum ℓ can be stated as $qr/\hbar > \ell$. Thus, one expects that quantum effects related to the angular momentum barrier to be important for $qr/\hbar$ near or below ℓ. Thus, quantum effects tend to damp out the kernel's resolving power for higher ℓ. Quantum tunneling through the Coulomb barrier is required when x, the ratio of the potential and kinetic energies defined in Eq. (14), exceeds unity. For identical pions, quantum effects associated with tunneling through the Coulomb barrier become important for $q < 10$ MeV/c.

Classically, the correlation function for charged particles is characterized by a scale $q_{\rm char}$ defined by $x \sim 1$.

$$q_{\rm char} = \sqrt{\frac{2\mu Z_1 Z_2 e^2}{r_{\rm char}}}, \tag{18}$$

where $r_{\rm char}$ is a characteristic size of the source. For pairs with a large reduced mass or charge, this characteristic scale is large. For instance, for Carbon-Carbon correlations, if $r_{\rm char} = 5$ fm, $q_{\rm char}$=340 MeV/c. For momentum in this range $qr/\hbar$ is large and the classical approximation is well justified. As a general rule, classical expressions for the Coulomb kernel work well for fragments larger than helium.

The right-hand side of Fig. 2 displays pK^+ kernels plotted for several values of ℓ as a function of r for $q = 75$ MeV/c. Kernels are shown for three cases. The first case takes into account only the Coulomb interaction and uses the

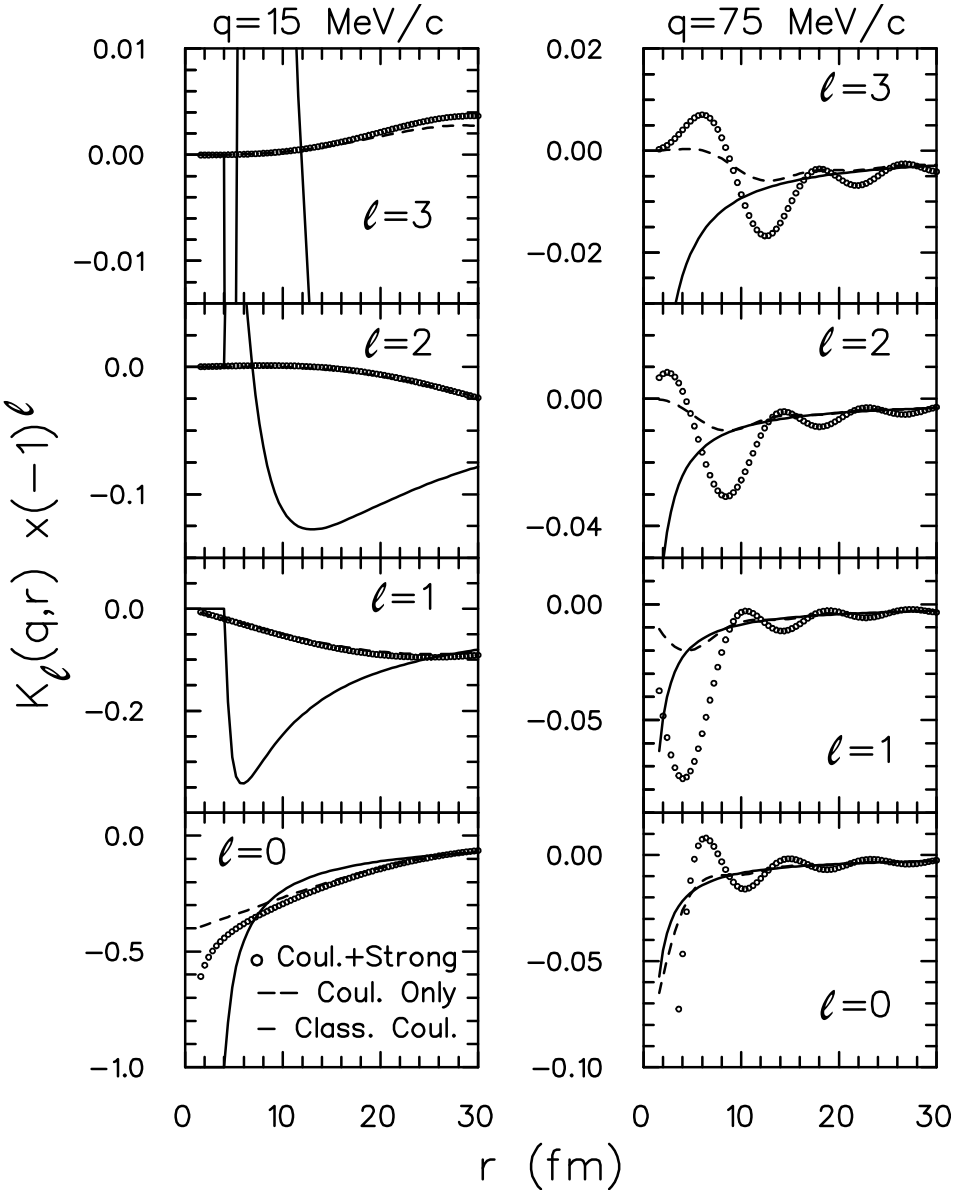

FIG. 2: Kernels for pK^+ interactions are shown for $q = 15$ MeV/c (left side) and $q = 75$ MeV/c (right panel) as a function of r for several values of ℓ. The classical approximation reproduces the quantum kernel with no strong interaction when qr is much larger than $(L + 1)\hbar$. Including the strong interaction results in oscillations.

classical expression for the squared wave function. The kernel falls of as $(-1)/(q^2 r)$ at large r and is independent of ℓ except at small relative momentum. The second case also considers only the Coulomb interaction but is constructed using the full Coulomb wavefunctions. These kernels mimic the classical expressions at large r but differ at small r where they approach zero as r^L. Whereas the classical results suggest that the resolving power of the Coulomb interaction is quasi-independent of ℓ, the inclusion of quantum effects shows that the kernel becomes less useful for higher ℓ due to the increasing importance of quantum smearing. To study the shape of $\mathcal{S}(\mathbf{r})$ at small scales, one must then study $\mathcal{R}(q)$ at large q where the correlation is unfortunately quite small. The third case displayed in Fig. (2) also takes into account the strong interaction between the protons and kaons. Although the phase shifts are not very large for pK^+ interactions, the strong interaction does generate a significant oscillation in $\mathcal{K}$. The next sub-section will focus on the effects of such interactions.

The left-side panels of Fig. 2 display the same kernels for $q = 15$ MeV/c. At small relative momentum, the quantum and classical calculations of $\mathcal{K}_\ell$ differ for the entire relative region of r. Furthermore, since phase shifts from the strong interaction tend to zero at $q = 0$, the strong interaction is not important in this case. Since quantum effects constrain the kernel to be near zero for $qr < L$, small values of q are not very useful for determining shape characteristics. For

sources where the characteristic size is near 5 fm, the best chance of learning shape information is for values of q between 30 and 100 MeV/c. For higher relative momentum, the correlation, which falls as $1/q^2$ might be too small to be accurately measured.

A peculiar aspect of the Coulomb kernel is that, though it is analytic as a function of r, it is not analytic as a function of q. Coulomb wave functions for a given partial wave can be expressed as,

$$\phi_\ell(q,r) = C_\ell(\eta)(qr)^{\ell+1}e^{-iqr}M(\ell+1-i\eta,2\ell+2,2iqr), \tag{19}$$

$$C_\ell(\eta) = 2^\ell e^{-\pi\eta/2}\frac{|\Gamma(\ell+1+i\eta)|}{\Gamma(2\ell+2)} \tag{20}$$

$$\eta = \frac{\mu e^2}{q}. \tag{21}$$

The non-analyticity is confined to the funtion $C_\ell(\eta)$, while the other factors, including the hyper-geometric function M, are analytic. One can divide the squared wave function by the Gamow factor,

$$G(\eta) \equiv e^{-\pi\eta}|\Gamma(1+i\eta)|^2 = \frac{2\pi\eta}{e^{2\pi\eta}-1}, \tag{22}$$

to find a quantity that is manifestly finite as $q \to 0$. However, even the "Gamow-corrected" kernel remains non-analytic, in that the higher ℓ pieces do not grow as q^ℓ. This follows from the fact that $\Gamma(\ell+1+i\eta) = (\ell+i\eta)\Gamma(\ell+i\eta)$, which provides an additional power of $1/q$ for each successively higher ℓ. This non-analyticity carries forward to the correlation functions. Thus, angular decompositions of Coulomb-driven correlation functions do not behave as q^ℓ at small q, even after Gamow correction.

Despite the complexity of the Coulomb wave function, one can easily summarize the resolving power of the Coulomb kernels. The Coulomb kernels provide an accurate means of measuring the expectation $Y_{\ell,m}/r$ by observing how $\mathcal{R}(q)$ approaches zero at large q,

$$\mathcal{R}_{\ell,m}(q\to\infty) \approx (4\pi)^{1/2}\frac{\mu e^2}{q^2}\left\langle \frac{1}{r}Y_{\ell,m}(\cos\theta_{qr})\right\rangle, \tag{23}$$

$$\mathcal{R}_{\bar{\ell}}(q\to\infty) \approx \frac{\mu e^2}{q^2}\left\langle \frac{1}{r}\mathcal{A}_{\bar{\ell}}(\Omega)\right\rangle. \tag{24}$$

Here, the averaging uses the source function as a weight,

$$\langle f\rangle = \int d^3r\mathcal{S}(\mathbf{r})f(\mathbf{r}). \tag{25}$$

Since the classical approximation is good for large qr, this relation is unchanged by quantum considerations. In the classical approximation one would be tempted to expand the kernel in powers of $2\mu e^2/(q^2r)$ and see that by expanding the measured correlation in powers of $1/q^2$ one could systematically identify the moments of the source distribution, $1/r$, $/r^2$, $1/r^3$. However, quantum effects alter the result as soon as one goes beyond the first moment.

C. Kernels from strong interactions

Strong interactions between two particles also provide leverage for extracting source information from measured correlations when the cross sections are large [22]. The distortion of the squared wave function from strong interactions can be divided into two categories. At small distances, less than one fm, the existence of a resonance results in a peak of the squared wave function. The short distance behavior is important for constructing the $\ell = 0$ kernel. However, the short distance behavior is irrelevant for affecting $\mathcal{R}^{(\ell)}$ for higher ℓ because $\mathcal{S}^{(\ell)}$ behaves as r^ℓ for small r. Since the principal motivation for this paper is to investigate what can be learned for $\ell > 0$, it is most important to understand the kernel at larger r where the wave function can be described by a distorted partial wave.

To investigate the structure of $\mathcal{K}_\ell$ at large r we first make a partial wave expansion. As $r \to \infty$.

$$\psi(q,r,\cos\theta_{qr}) \sim \frac{1}{2iqr}\sum_{\ell''}(2\ell''+1)P_{\ell''}(\cos\theta_{qr})\left(e^{iqr}-(-1)^{\ell''}e^{-iqr}\right)+\delta\psi, \tag{26}$$

$$\delta\psi = \frac{e^{iqr}}{qr}\sum_{\ell'}(2\ell'+1)e^{i\delta_{\ell'}}\sin\delta_{\ell'}P_{\ell'}(\cos\theta_{qr}). \tag{27}$$

Squaring the wave function,

$$\begin{aligned}|\psi(q,r,\Omega)|^2-1 &\sim \frac{1}{r^2}\frac{d\sigma}{d\Omega}-\frac{\sigma_{\rm tot}}{r^2}\delta(\Omega) \\ &+\frac{1}{(qr)^2}\sum_{\ell',\ell''}(2\ell'+1)(2\ell''+1)P_{\ell'}(\cos\theta_{qr})P_{\ell''}(\cos\theta_{qr})(-1)^{\ell'}\sin\delta_{\ell'}\sin(2qr+\delta_{\ell'}), \\ \sigma_{\rm tot} &= \frac{4\pi}{q^2}\sum_{\ell'}(2\ell'+1)\sin^2\delta_{\ell'}, \\ \frac{d\sigma}{d\Omega} &= \frac{1}{q^2}\left|\sum_{\ell'}e^{i\delta_{\ell'}}\sin\delta_{\ell'}P_{\ell'}(\cos\theta_{qr}).\right|^2\end{aligned} \tag{28}$$

The first term describes the scattering of particles into the direction $\vec{\Omega}$, while the second term describes the loss of flux in the forward direction where $\delta(\Omega)$ is zero for $\cos\theta\neq 1$ and $\int d\Omega\delta(\Omega)=1$. The final term represents an interference term which can be neglected in the classical limit due to the oscillation with r.

In order to calculate the Kernel, we re-express $d\sigma/d\Omega$ in Eq. (28) in terms of Legendre polynomials,

$$\begin{aligned}|\psi(q,r,\Omega)|^2 &= \frac{1}{(qr)^2}\sum_{\ell',\ell''}(2\ell''+1)(2\ell'+1)P_{\ell'}(\cos\theta_{qr})P_{\ell''}(\cos\theta_{qr})\left[\sin\delta_{\ell'}\sin\delta_{\ell''}+(-1)^{\ell'}\sin\delta_{\ell'}\sin(2qr+\delta_{\ell'})\right] \\ &-\frac{\sigma_{\rm tot}}{r^2}\delta(\Omega).\end{aligned} \tag{29}$$

When calculating $\mathcal{K}_\ell(q,r)$ one needs to integrate the product of 3 Legendre polynomials.

$$J_{\ell'',\ell',\ell} \equiv \int_{-1}^{1}dx P_{\ell''}(x)P_{\ell'}(x)P_\ell(x) \tag{30}$$

$$= \frac{1}{\pi}\frac{[(\ell''+\ell'+\ell)/2]!\Gamma([-\ell''+\ell'+\ell+1]/2)\Gamma([\ell''-\ell'+\ell+1]/2)\Gamma([\ell''+\ell'-\ell+1]/2)}{\Gamma([\ell''+\ell'+\ell+3]/2)[(-\ell''+\ell'+\ell)/2]![(\ell''-\ell'+\ell)/2]![(\ell''+\ell'-\ell)/2]!}, \tag{31}$$

when none of the three angular momenta are larger than the sum of the other two. Otherwise, $J=0$. Writing $\mathcal{K}_\ell$ in terms of the phase shifts and J,

$$\mathcal{K}_\ell(q,r)=\frac{1}{2(qr)^2}\sum_{\ell',\ell''}(2\ell'+1)(2\ell''+1)J_{\ell'',\ell',\ell}\left[\sin\delta_{\ell'}\sin\delta_{\ell''}+(-1)^{\ell'}\sin\delta_{\ell'}\sin(2qr+\delta_{\ell'})\right]-\frac{\sigma_{\rm tot}}{4\pi r^2}. \tag{32}$$

The $\ell=0$ piece is particularly interesting. Using the identity, $J_{\ell',\ell'',0}=2\delta_{\ell',\ell''}/(2\ell'+1)$, one can see that the first and last term cancel giving,

$$K_{\ell=0}(q,r)=\frac{1}{(qr)^2}\sum_{\ell'}(2\ell'+1)(-1)^{\ell'}\sin\delta_{\ell'}\sin(2qr+\delta_{\ell'}). \tag{33}$$

The reason the non-oscillating terms vanish reflects the fact that in the classical limit particles scatter from the potential, but the scattering does not increase the probability of observing particles asymptotically with momenta of magnitude q since the kinetic energy not changed by the potential since they originate at large r where the potential is zero. This is different than the Coulomb case where the potential is long range and the momenta are affected out to arbitrary r.

For ℓ much larger than the angular momenta for which phase shifts are non-zero, only the last term in Eq. (32) remains. This term represents the spherical harmonic decomposition of the delta function describing the shadowing at $\cos\theta_{qr}=1$. Thus, even for purely s-wave scattering the shadowing term provides leverage to investigate characteristics of the source for all ℓ. The discriminating power falls as $1/r^2$ and is proportional to the cross section. Thus, when looking for shape, one has the best chance of looking for values of q near a resonance since the cross sections are large. Since cross sections also tend to be large at low q, modest phase shifts can be exploited near threshold, though one must remember that for small q, the expansion in $1/r$ discussed here is not valid.

III. CARTESIAN HARMONICS

Here, we briefly describe the nature of Cartesian harmonics before giving a more in-depth description of the mathematical properties in the next two sub-sections. Cartesian harmonics can play the same role as spherical

TABLE I: Cartesian harmonics for $\ell <= 4$. Other harmonics can be found by either permuting the indices, e.g., $\mathcal{A}_{xyx} = \mathcal{A}_{xxy}$, or by swapping indices on both sides of the equation, e.g., $x \leftrightarrow y$. For example, given $\mathcal{A}_{xxy} = n_x^2 n_y - n_y/5$, swapping $y \leftrightarrow z$ gives $\mathcal{A}_{xxz} = n_x^2 n_z - n_z/5$.

$\mathcal{A}_x^{(1)} = n_x$	$\mathcal{A}_{xyz}^{(3)} = n_x n_y n_z$
$\mathcal{A}_{xx}^{(2)} = n_x^2 - (1/3)$	$A_{xxxx}^{(4)} = n_x^4 - (6/7)n_x^2 + (3/35)$
$\mathcal{A}_{xy}^{(2)} = n_x n_y$	$\mathcal{A}_{xxxy}^{(4)} = n_x^3 n_y - (3/7)n_x n_y$
$A_{xxx}^{(3)} = n_x^3 - (3/5)n_x$	$\mathcal{A}_{xxyy}^{(4)} = n_x^2 n_y^2 - (1/7)n_x^2 - (1/7)n_y^2 + (1/35)$
$\mathcal{A}_{xxy}^{(3)} = n_x^2 n_y - (1/5)n_y$	$\mathcal{A}_{xxyz}^{(4)} = n_x^2 n_y n_z - (1/7)n_y n_z$

harmonics as they can serve as the basis for expressing the angular information contained in a function $F(\Omega)$ with an array of coefficients,

$$F(\Omega) = \sum_{\ell_x,\ell_y,\ell_z} \gamma(\vec{\ell}) F_{\vec{\ell}}\, n_x^{\ell_x} n_y^{\ell_y} n_z^{\ell_z}, \tag{34}$$

$$\gamma(\vec{\ell}) \equiv \frac{\ell!}{\ell_x!\ell_y!\ell_z!}, \tag{35}$$

where $\hat{n}$ is a unit vector and $\ell \equiv \ell_x + \ell_y + \ell_z$. This representation can be used either for correlation functions, where a different array of coefficients is used for each value of relative momentum q, or for source functions, where one would assign an array for each bin in the radius r. The advantage of Cartesian harmonics is that the coefficients $F_{\vec{\ell}}$ provide a more direct physical understanding of the shape than do the complex coefficients $F_{\ell,m}$ used when expanding with spherical harmonics.

The coefficients $F_{\vec{\ell}}$ can be generated from $F(\Omega)$ through convolution with the Cartesian harmonic functions $A_{\vec{\ell}}(\Omega)$,

$$F_{\vec{\ell}} = \frac{(2\ell+1)!!}{\ell!} \int \frac{d\Omega}{4\pi} F(\Omega) \mathcal{A}_{\vec{\ell}}(\Omega). \tag{36}$$

The functions $\mathcal{A}_{\vec{\ell}}(\Omega)$ are most readily expressed in terms of unit vector components. Each function can be written as $n_x^{\ell_x} n_y^{\ell_y} n_z^{\ell_z}$ plus terms of lower power of ℓ. Examples appear in Table I. As an alternative notation, the arrays of coefficients, or the Cartesian harmonic functions themselves, are often labeled as if they were an ℓ^{th} rank tensor, $F^{(\ell)}_{\alpha_1\cdots\alpha_\ell}$. For instance, $F_{\ell_x=2,\ell_y=1,\ell_z=1} \leftrightarrow F^{(4)}_{xxyz}$. This equivalence in notation stems from the fact that the tensor F is symmetric with respect to permutation of the indices which allows one to refer to any element of the tensor by the number of occurences of each index.

In addition to being symmetric, the tensor of expansion coefficients is also traceless,

$$\sum_\beta F^{(\ell)}_{\alpha_1\cdots\alpha_{\ell-2},\beta,\beta} = 0 \tag{37}$$

$$F_{\ell_x+2,\ell_y,\ell_z} + F_{\ell_x,\ell_y+2,\ell_z} + F_{\ell_x,\ell_y,\ell_z+2} = 0.$$

Whereas a symmetric tensor of rank ℓ has $(\ell+1)(\ell+2)/2$ independent components, the tracelessness condition reduces the number of independent components to $(2\ell+1)$. For instance, for a given ℓ, if one knows the $(2\ell+1)$ coefficients for $\ell_x = 0, 1$, $F_{(\ell_x=0,1),\ell_y,\ell_z}$, the remaining coefficients can be generated with Eq. (37). As described in the following subsection, these coefficients can be expressed in terms of coefficients for expanding with spherical harmonics of the same ℓ. When expanding with spherical harmonics, one uses $(2\ell+1)$ complex coefficients $F_{\ell,m}$, but since the $(\ell = 0, m = 0)$ coefficient is real, and since the $F_{\ell,-m} = (-1)^m F^*_{\ell,m}$, the number of independent real numbers required to represent $F_{\ell,m}$ is also $(2\ell+1)$.

A. Mathematical Properties and Relation to Symmetric Traceless Tensors

The properties of Cartesian Harmonics or the arrays used to store expansion coefficients are closely related to the properties of ℓ^{th} rank symmetric tensors. This relation stems from the fact that symmetric traceless tensors can be used to express arbitrary solutions to the Laplace equation. If one considers a function,

$$F(\mathbf{r}) = \sum_{\ell,\alpha_1\cdots\alpha_\ell} F^{(\ell)}_{\alpha_1\cdots\alpha_\ell} r_{\alpha_1}\cdots r_{\alpha_\ell} \tag{38}$$

$$= \sum_{\vec{\ell}} \gamma(\vec{\ell}) F_{\vec{\ell}} x^{\ell_x} y^{\ell_y} z^{\ell_z}, \tag{39}$$

the Laplace equation,

$$\begin{aligned}\nabla^2 F(\mathbf{r}) &= 0 \\ &= \sum_{\vec{\ell}} \frac{(\ell+2)!}{\ell!}\gamma(\vec{\ell})\left[F_{\ell_x+2,\ell_y,\ell_z} + F_{\ell_x,\ell_y+2,\ell_z} + F_{\ell_x,\ell_y,\ell_z+2}\right] x^{\ell_x} y^{\ell_y} z^{\ell_z},\end{aligned} \tag{40}$$

will be satisfied if F obeys the tracelessness constraint, Eq. (37).

Any symmetric tensor of a given rank ℓ, $M^{(\ell)}$, can be expressed in terms of traceless tensors of equal or lower rank, $\tilde{M}^{(\ell')}$, where $\ell' = \ell, \ell-2, \ell-4\cdots$.

$$M^{(\ell)}_{\alpha_1\cdots\alpha_\ell} = \sum_{\ell'=\ell,\ell-2\cdots} S^{(2\ell)}_{\alpha_1\cdots\alpha_\ell,\alpha'_1\cdots\alpha'_{\ell'}} \delta_{\alpha'_1,\alpha'_2}\cdots\delta_{\alpha'_{\ell-\ell'-1},\alpha_{\ell-\ell'}} \tilde{M}^{(\ell')}_{\alpha_{\ell-\ell'+1}\cdots\alpha_\ell}, \tag{41}$$

$$M^{(\ell)} = \sum_{\ell'=\ell,\ell-2\cdots} S\cdot\left[(\delta^{(2)}\otimes)^{(\ell-\ell')/2}\tilde{M}^{(\ell')}\right] \tag{42}$$

where S is the symmetrization tensor which is $1/\ell!$ if the indices α' are a permutation of α and is zero otherwise. One can find the tensors $\tilde{M}^{(\ell')}$ recursively from $M^{(\ell)}$. First, one can take the trace $\ell/2$ times, to provide $\tilde{M}^{(\ell'=0)}$ or $\tilde{M}^{(\ell'=1)}$ depending on whether ℓ' is even or odd. One can then subtract away the contribution of the lowest order from $M^{(\ell)}$ to find a tensor with no components with $\ell' \le 1$. One can then repeat the procedure, taking a trace $\ell/2-1$ times to find the next highest tensor $\tilde{M}^{(\ell=2 \text{ or } 3)}$. Since the procedure is linear, and since $\tilde{M} = M$ if M is traceless, one may describe the procedure with linear operators P,

$$\tilde{M}^{(\ell')}_{\alpha'_1\cdots\alpha'_{\ell'}} = \sum_{\alpha_1\cdots\alpha_\ell} P^{(\ell'+\ell)}_{\alpha'_1\cdots\alpha_{\ell'},\alpha_1\cdots\alpha_\ell}(\ell',\ell) M^{(\ell)}_{\alpha_1\cdots\alpha_\ell}. \tag{43}$$

The projection $P^{(\ell')}_{\vec{\ell}',\vec{\ell}}(\ell'=\ell,\ell)$ is symmetric with respect to the interchange of $\vec{\ell}$ and $\vec{\ell}'$, and satisfies the conditions for projection operators,

$$\sum_{\alpha'_1\cdots\alpha'_\ell} P^{(2\ell)}_{\alpha_1\cdots\alpha_\ell,\alpha'_1\cdots\alpha'_\ell}(\ell,\ell) P^{(2\ell)}_{\alpha'_1\cdots\alpha'_\ell,\alpha''_1\cdots\alpha''_\ell}(\ell,\ell) = P^{(2\ell)}_{\alpha_1\cdots\alpha_\ell,\alpha''_1\cdots\alpha''_\ell}(\ell,\ell). \tag{44}$$

The lower-rank operators $P^{(\ell'+\ell)}(\ell' < \ell,\ell)$ can also be used to define projection operators, as $S\cdot[(\delta^{(2)}\otimes)^{(\ell-\ell')/2}P^{(\ell'+\ell)}(\ell'<\ell,\ell)$ also satisfies the properties of a projection operator. The projection for $\ell' = \ell$ can also be written in terms of operators of lower rank,

$$\begin{aligned}P^{(\ell'+\ell)}_{\alpha'_1\cdots\alpha'_\ell,\alpha_1\cdots\alpha_\ell}(\ell'=\ell,\ell) &= S^{(2\ell)}_{\alpha'_1\cdots\alpha'_\ell,\alpha_1\cdots\alpha_\ell} \\ &\quad - \sum_{\alpha''_1\cdots\alpha''_{\ell''},\ell''<\ell} S^{(2\ell)}_{\alpha'_1\cdots\alpha'_\ell,\alpha''_1\cdots\alpha''_{\ell''}}\delta_{\alpha''_1,\alpha''_2}\cdots\delta_{\alpha''_{\ell-\ell''-1},\alpha''_{\ell-\ell''}} P^{(\ell+\ell'')}_{\alpha''_{\ell-\ell''+1}\cdots\alpha''_\ell,\alpha_1\cdots\alpha_\ell}(\ell'',\ell).\end{aligned} \tag{45}$$

The first term acts like the identity operator when operating on a symmetric tensor.

The projection operator $P^{(2\ell)}_{\alpha'_1\cdots\alpha'_\ell,\alpha_1\cdots\alpha_\ell}(\ell'=\ell,\ell)$ satisfies the tracelessness condition for both the α and α' indices. This means that the function

$$\begin{aligned}F^{(\ell)}_{\alpha_1\cdots\alpha_\ell}(\mathbf{r}) &\equiv \sum_{\alpha'_1,\alpha'_\ell} P^{(2\ell)}_{\alpha_1\cdots\alpha_\ell,\alpha'_1\cdots\alpha'_\ell}(\ell,\ell'=\ell) r_{\alpha'_1}\cdots r_{\alpha'_\ell} \\ &= \sum_{\vec{\ell}'}\gamma(\vec{\ell}')P_{\vec{\ell},\vec{\ell}'}(\ell,\ell'=\ell) n_x^{\ell'_x} n_y^{\ell'_y} n_z^{\ell'_z}\end{aligned} \tag{46}$$

satisfies the Laplace equation. By replacing x, y and z with components of a unit vector, one finds a solution of the angular part of the Laplace equation,

$$\mathcal{A}_{\vec{\ell}}(\hat{n}) \equiv \sum_{\vec{\ell}',\ell'=\ell}\gamma(\vec{\ell}')P_{\vec{\ell},\vec{\ell}'}(\ell,\ell) n_x^{\ell'_x} n_y^{\ell'_y} n_z^{\ell'_z} \tag{47}$$

$$\left[\frac{1}{\sin\theta}\frac{\partial}{\partial\theta}\left(\sin\theta\frac{\partial}{\partial\theta}\right) + \frac{1}{\sin^2\theta}\frac{\partial^2}{\partial\phi^2}\right]\mathcal{A}_{\vec{\ell}}(\hat{n}) = -\ell(\ell+1)\mathcal{A}_{\vec{\ell}}(\hat{n}). \tag{48}$$

These solutions are referred to as Cartesian harmonics.

If one writes the projection operator in Eq. (47) as $\delta_{\vec{\ell},\vec{\ell}'}$ minus a sum over projections of lower rank as shown in Eq. (45), one can use the fact that the lower-rank terms in Eq. (45) have at least one delta function to state that Cartesian harmonics $\mathcal{A}_{\vec{\ell}}$ can be written as a product $n_x^{\ell_x} n_y^{\ell_y} n_z^{\ell_z}$ plus other terms where the unit vector components appear in powers $\ell-2, \ell-4 \cdots$. A closed-form expression is given in [24],

$$\begin{aligned} \mathcal{A}_{\vec{\ell}} &= \sum_{\vec{m}=0, m_i \le \ell_i/2} \left(\frac{-1}{2}\right)^m \frac{(2\ell-2m-1)!!}{(2\ell-1)!!} \\ &\times \frac{\ell_x!}{(\ell_x-2m_x)!m_x!} \frac{\ell_y!}{(\ell_y-2m_y)!m_y!} \frac{\ell_z!}{(\ell_z-2m_z)!m_z!} n_x^{\ell_x-2m_x} n_y^{\ell_y-2m_y} n_z^{\ell_z-2m_z}, \end{aligned} \tag{49}$$

where $m = m_x + m_y + m_z$ and $(-1)! = 1$. Examples for a few cases of lower ℓ are shown in Table I. They can also be generated recursively [25], beginning with $\mathcal{A}^{(\ell=0)} = 1$,

$$\begin{aligned} \mathcal{A}^{(\ell)}_{\alpha_1 \cdots \alpha_\ell} &= \frac{1}{\ell} \sum_i n_{\alpha_i} \mathcal{A}^{(\ell-1)}_{\alpha_1 \cdots \alpha_{i-1} \alpha_{i+1} \cdots \alpha_\ell} \\ &- \frac{2}{\ell(2\ell-1)} \sum_{i<j} \sum_\alpha \delta_{\alpha_i,\alpha_j} n_\alpha \mathcal{A}^{(\ell-1)}_{\alpha,\alpha_1 \cdots \alpha_{i-1} \alpha_{i+1} \cdots \alpha_{j-1} \alpha_{j+1} \cdots \alpha_\ell}. \end{aligned} \tag{50}$$

Expressions for several Cartesian harmonics are given in Table I. One of the properties of Cartesian harmonics is that, unlike with spherical harmonics where the z axis is singled out to define the angles, the three axes are treated equally.

For a fixed ℓ, there are $(\ell+1)(\ell+2)/2$ different functions $A_{\vec{\ell}}$, but the tracelessness condition,

$$\mathcal{A}_{\ell_x+2,\ell_y,\ell_z} = -\mathcal{A}_{\ell_x,\ell_y+2,\ell_z} - \mathcal{A}_{\ell_x,\ell_y,\ell_z+2}, \tag{51}$$

allows one to generate all harmonics for $\ell_x > 1$ from the harmonics for $\ell_x = 0$ and $\ell_x = 1$.

These $(2\ell+1)$ solutions form a complete set for spanning angular degrees of freedom. To derive a completeness relation, we first note that Cartesian harmonics for all the indices along the z-axis can be expressed in terms of Legendre Polynomials,

$$\mathcal{A}_{\ell_z=\ell,\ell_x=0,\ell_y=0}(\hat{n}) = \frac{\ell!}{(2\ell-1)!!} P_\ell(n_z) \tag{52}$$

$$= \sum_{\alpha_1 \cdots \alpha_\ell, \alpha'_1 \cdots \alpha'_\ell} \hat{e}_{\alpha_1} \cdots \hat{e}_{\alpha_\ell} P^{(2\ell)}_{\alpha_1 \cdots \alpha_\ell, \alpha'_1 \cdots \alpha'_\ell}(\ell,\ell) n_{\alpha'_1} \cdots n_{\alpha'_\ell}, \tag{53}$$

$$\tag{54}$$

where $\hat{e}$ is a unit vector along the z axis. Making use of the fact that $P(\ell,\ell)$ is a projection operator, $\hat{e}^\ell P^{(2\ell)} \hat{n}^\ell = \hat{e}^\ell P^{(2\ell)} P^{(2\ell)} \hat{n}^\ell$, one can transform the completeness relation for spherical harmonics into a completeness relation for Cartesian harmonics [25],

$$\delta(\Omega - \Omega') = \sum_\ell \frac{(2\ell+1)}{4\pi} P_\ell(\hat{n} \cdot \hat{n}') \tag{55}$$

$$= \frac{1}{4\pi} \sum_\ell \frac{(2\ell+1)!!}{\ell!} \sum_{\alpha_1 \cdots \alpha_\ell} \mathcal{A}^{(\ell)}_{\alpha_1 \cdots \alpha_\ell}(\hat{n}) \mathcal{A}^{(\ell)}_{\alpha_1 \cdots \alpha_\ell}(\hat{n}') \tag{56}$$

$$= \frac{1}{4\pi} \sum_{\vec{\ell}} \frac{(2\ell+1)!!}{\ell!} \gamma(\vec{\ell}) \mathcal{A}_{\vec{\ell}}(\Omega') \mathcal{A}_{\vec{\ell}}(\Omega) \tag{57}$$

$$= \frac{1}{4\pi} \sum_{\vec{\ell}} \frac{(2\ell+1)!!}{\ell!} \gamma(\vec{\ell}) \mathcal{A}^{(\ell)}_{\vec{\ell}}(\Omega') n_x^{\ell_x} n_y^{\ell_y} n_z^{\ell_z}.$$

Here, the last step involved applying the condition that $\mathcal{A}_{\vec{\ell}}$ can be expressed using the projector as defined in Eq. (45). The only term which survives contraction with a traceless tensor is the first term which has no delta function. Using the completeness relation, one can derive Eq. (34) which provides an angular function $F(\Omega)$ given the coefficients $F_{\vec{\ell}}$ defined in Eq. (36).

One can also generate the unit-vector moments from the harmonics of equal and lower order,

$$n_x^{\ell_x} n_y^{\ell_y} n_z^{\ell_z} = \sum_{\vec{m}=0, m_i \le \ell_i/2} \left(\frac{1}{2}\right)^m \frac{(2\ell - 4m + 1)!!}{(2\ell - 2m + 1)!!} \times \frac{\ell_x!}{(\ell_x - 2m_x)! m_x!} \frac{\ell_y!}{(\ell_y - 2m_y)! m_y!} \frac{\ell_z!}{(\ell_z - 2m_z)! m_z!} \mathcal{A}_{\vec{\ell} - 2\vec{m}}. \tag{58}$$

This expression allows one to calculate Cartesian moments of distributions if given the decomposition into Cartesian harmonics. For example, after decomposing the source function with Cartesian harmonics, the moments of the source function become,

$$\int d^3 r \mathcal{S}(\mathbf{r}) r_x^{\ell_x} r_y^{\ell_y} r_z^{\ell_z} = \frac{\ell!}{(2\ell+1)!!} \sum_{\vec{m}=0, m_i \le \ell_i/2} \left(\frac{1}{2}\right)^m \frac{(2\ell - 4m + 1)!!}{(2\ell - 2m + 1)!!} \times \frac{\ell_x!}{(\ell_x - 2m_x)! m_x!} \frac{\ell_y!}{(\ell_y - 2m_y)! m_y!} \frac{\ell_z!}{(\ell_z - 2m_z)! m_z!} 4\pi \int dr r^{\ell+2} \mathcal{S}_{\vec{\ell} - 2\vec{m}}(r). \tag{59}$$

Cartesian harmonics are orthogonal to one another if they come from different multiplets ℓ, or if any of the subscripts ℓ_i differ by an odd number. Otherwise, the orthonormality relations are given by [24],

$$\langle \vec{\ell} | \vec{\ell}' \rangle \equiv \int d\Omega \mathcal{A}_{\vec{\ell}} \mathcal{A}_{\vec{\ell}'} = \frac{4\pi}{(2\ell+1)} \frac{1}{[(2\ell-1)!!]^2} \delta_{\ell,\ell'} \sum_{\vec{m}=0, m_i \le \ell_i/2} \left(\frac{-1}{2}\right)^m m! (2\ell - 2m - 1)!! \times \prod_{i=x,y,z} \frac{\ell_i! \ell_i'!}{((\ell_i' - \ell_i)/2 + m_i)! (\ell_i - 2m_i)! m_i!} \Theta((\ell_i' - \ell_i)/2 + m_i), \tag{60}$$

where $\Theta(n)$ is unity if $n \ge 0$ and is zero for negative n.

For completeness, we provide expressions shown in [24] for spherical harmonics in terms of Cartesian harmonics,

$$Y_{\ell,m} = (-1)^m (2\ell - 1)!! \left[\frac{2\ell+1}{4\pi(\ell+m)!(\ell-m)!}\right]^{1/2} \sum_{k=0}^{m} i^{(m-k)} \frac{m!}{(m-k)! k!} \mathcal{A}_{[k, m-k, \ell-m]}. \tag{61}$$

The inverse transformations, also from [24], are more complicated.

$$\mathcal{A}_{\vec{\ell}} = (2\ell - 1)!! \sum_{m=-\ell}^{\ell} (-1)^m \left[\frac{2\ell+1}{4\pi(\ell+m)!(\ell-m)!}\right]^{1/2} \sum_{k=0}^{m} (-i)^{(m-k)} \frac{m!}{k!(m-k)!} \times \langle \vec{\ell} | [k, m-k, \ell-m] \rangle Y_{\ell,m}, \tag{62}$$

where a closed expression for the overlap integral is given in Eq. (60). Transformations between spherical and Cartesian harmonics are listed in Table II for $\ell \le 4$.

B. Multiplying, Dividing and Inverting Cartesian Arrays

Often one wishes to multiply or divide angular functions. For instance, for correlation functions,

$$X(\Omega) = B(\Omega) C(\Omega), \tag{63}$$

where $X(\Omega)$ could be a two-particle distribution for a given relative momentum q, $B(\Omega)$ could be a mixed-event (or background) distribution and $C(\Omega)$ would be the correlation function. If one performed a two-dimensional binning in $\cos\theta$ and ϕ, one could find $C(\Omega)$ by dividing X by B for each bin. However, if one wants to expand C in Cartesian harmonics, the result could be distorted by residual binning effects which would disappear in the limit of fine binning, but requires high statistics.

An alternative approach is to explicitly solve for the coefficients $C_{\vec{\ell}}$ given $X_{\vec{\ell}}$ and $B_{\vec{\ell}}$. One advantage of this approach is that one could forego binning in terms of $\cos\theta$ and ϕ. For instance, when reading in the values for the distribution X, one could increment the array for each bin $\vec{\ell}$ by an amount $[(2\ell+1)!!/\ell!]\mathcal{A}_{\vec{\ell}}(\hat{q})$ as described by Eq. (36) to yield

TABLE II: Transformations between Cartesian and spherical harmonics

$$Y_{1,0} = (1/2)\sqrt{3/\pi}\mathcal{A}_z^{(1)}$$
$$Y_{1,\pm1} = -(i/2)\sqrt{3/2\pi}\mathcal{A}_y^{(1)} \mp (1/2)\sqrt{3/2\pi}\mathcal{A}_x^{(1)}$$
$$Y_{2,0} = (3/4)\sqrt{5/\pi}\mathcal{A}_{zz}^{(2)}$$
$$Y_{2,\pm1} = -(i/2)\sqrt{15/2\pi}\mathcal{A}_{yz}^{(2)} \mp (1/2)\sqrt{15/2\pi}\mathcal{A}_{xz}^{(2)}$$
$$Y_{2,\pm2} = -(1/4)\sqrt{15/2\pi}\mathcal{A}_{yy}^{(2)} \pm (i/2)\sqrt{15/2\pi}\mathcal{A}_{xy}^{(2)} + (1/4)\sqrt{15/2\pi}\mathcal{A}_{xx}^{(2)}$$
$$Y_{3,0} = (5/4)\sqrt{7/\pi}\mathcal{A}_{zzz}^{(3)}$$
$$Y_{3,\pm1} = -(5i/8)\sqrt{21/\pi}\mathcal{A}_{yzz}^{(3)} \mp (5/8)\sqrt{21/\pi}\mathcal{A}_{xzz}^{(3)}$$
$$Y_{3,\pm2} = -(1/4)\sqrt{105/2\pi}\mathcal{A}_{yyz}^{(3)} \pm (i/2)\sqrt{105/2\pi}\mathcal{A}_{xyz}^{(3)} + (1/4)\sqrt{105/2\pi}\mathcal{A}_{xxz}^{(3)}$$
$$Y_{3,\pm3} = (i/8)\sqrt{35/\pi}\mathcal{A}_{yyy}^{(3)} \pm (3/8)\sqrt{35/\pi}\mathcal{A}_{xyy}^{(3)} - (3i/8)\sqrt{35/\pi}\mathcal{A}_{xxy}^{(3)} \mp (1/8)\sqrt{35/\pi}\mathcal{A}_{xxx}^{(3)}$$
$$Y_{4,0} = (105/16)\sqrt{1/\pi}\mathcal{A}_{zzzz}^{(4)}$$
$$Y_{4,\pm1} = -(21i/8)\sqrt{5/\pi}\mathcal{A}_{yzzz}^{(4)} \mp (21/8)\sqrt{5/\pi}\mathcal{A}_{xzzz}^{(4)}$$
$$Y_{4,\pm2} = -(21/8)\sqrt{5/2\pi}\mathcal{A}_{yyzz}^{(4)} \pm (21i/4)\sqrt{5/2\pi}\mathcal{A}_{xyzz}^{(4)} + (21/8)\sqrt{5/2\pi}\mathcal{A}_{xxzz}^{(4)}$$
$$Y_{4,\pm3} = (3i/8)\sqrt{35/\pi}\mathcal{A}_{yyyz}^{(4)} \pm (9/8)\sqrt{35/\pi}\mathcal{A}_{xyyz}^{(4)} - (9i/8)\sqrt{35/\pi}\mathcal{A}_{xxyz}^{(4)} \mp (3/8)\sqrt{35/\pi}\mathcal{A}_{xxxz}^{(4)}$$
$$Y_{4,\pm4} = (3/16)\sqrt{35/2\pi}\mathcal{A}_{yyyy}^{(4)} \mp (3i/4)\sqrt{35/2\pi}\mathcal{A}_{xyyy}^{(4)} - (9/8)\sqrt{35/2\pi}\mathcal{A}_{xxyy}^{(4)} \pm (3i/4)\sqrt{35/2\pi}\mathcal{A}_{xxxy}^{(4)} + (3/16)\sqrt{35/2\pi}\mathcal{A}_{xxxx}^{(4)}$$

$$\mathcal{A}_z^{(1)} = 2\sqrt{\pi/3}Y_{1,0}$$
$$\mathcal{A}_y^{(1)} = i\sqrt{2\pi/3}Y_{1,1} + i\sqrt{2\pi/3}Y_{1,-1}$$
$$\mathcal{A}_x^{(1)} = -\sqrt{2\pi/3}Y_{1,1} + \sqrt{2\pi/3}Y_{1,-1}$$
$$\mathcal{A}_{zz}^{(2)} = (4/3)\sqrt{\pi/5}Y_{2,0}$$
$$\mathcal{A}_{yz}^{(2)} = i\sqrt{2\pi/15}Y_{2,1} + i\sqrt{2\pi/15}Y_{2,-1}$$
$$\mathcal{A}_{yy}^{(2)} = -\sqrt{2\pi/15}Y_{2,2} - (2/3)\sqrt{\pi/5}Y_{2,0} - \sqrt{2\pi/15}Y_{2,-2}$$
$$\mathcal{A}_{xz}^{(2)} = -\sqrt{2\pi/15}Y_{2,1} + \sqrt{2\pi/15}Y_{2,-1}$$
$$\mathcal{A}_{xy}^{(2)} = -i\sqrt{2\pi/15}Y_{2,2} + i\sqrt{2\pi/15}Y_{2,-2}$$
$$\mathcal{A}_{xx}^{(2)} = \sqrt{2\pi/15}Y_{2,2} - (2/3)\sqrt{\pi/5}Y_{2,0} + \sqrt{2\pi/15}Y_{2,-2}$$
$$\mathcal{A}_{zzz}^{(3)} = (4/5)\sqrt{\pi/7}Y_{3,0}$$
$$\mathcal{A}_{yzz}^{(3)} = (4i/5)\sqrt{\pi/21}Y_{3,1} + (4i/5)\sqrt{\pi/21}Y_{3,-1}$$
$$\mathcal{A}_{yyz}^{(3)} = -\sqrt{2\pi/105}Y_{3,2} - (2/5)\sqrt{\pi/7}Y_{3,0} - \sqrt{2\pi/105}Y_{3,-2}$$
$$\mathcal{A}_{yyy}^{(3)} = -i\sqrt{\pi/35}Y_{3,3} - (i/5)\sqrt{3\pi/7}Y_{3,1} - (i/5)\sqrt{3\pi/7}Y_{3,-1} - i\sqrt{\pi/35}Y_{3,-3}$$
$$\mathcal{A}_{xzz}^{(3)} = -(4/5)\sqrt{\pi/21}Y_{3,1} + (4/5)\sqrt{\pi/21}Y_{3,-1}$$
$$\mathcal{A}_{xyz}^{(3)} = -i\sqrt{2\pi/105}Y_{3,2} + i\sqrt{2\pi/105}Y_{3,-2}$$
$$\mathcal{A}_{xyy}^{(3)} = \sqrt{\pi/35}Y_{3,3} + (1/5)\sqrt{\pi/21}Y_{3,1} - (1/5)\sqrt{\pi/21}Y_{3,-1} - \sqrt{\pi/35}Y_{3,-3}$$
$$\mathcal{A}_{xxz}^{(3)} = \sqrt{2\pi/105}Y_{3,2} - (2/5)\sqrt{\pi/7}Y_{3,0} + \sqrt{2\pi/105}Y_{3,-2}$$
$$\mathcal{A}_{xxy}^{(3)} = i\sqrt{\pi/35}Y_{3,3} - (i/5)\sqrt{\pi/21}Y_{3,1} - (i/5)\sqrt{\pi/21}Y_{3,-1} + i\sqrt{\pi/35}Y_{3,-3}$$
$$\mathcal{A}_{xxx}^{(3)} = -\sqrt{\pi/35}Y_{3,3} + (1/5)\sqrt{3\pi/7}Y_{3,1} - (1/5)\sqrt{3\pi/7}Y_{3,-1} + \sqrt{\pi/35}Y_{3,-3}$$
$$\mathcal{A}_{zzzz}^{(4)} = (16/105)\sqrt{\pi}Y_{4,0}$$
$$\mathcal{A}_{yzzz}^{(4)} = (4i/21)\sqrt{\pi/5}Y_{4,1} + (4i/21)\sqrt{\pi/5}Y_{4,-1}$$
$$\mathcal{A}_{yyzz}^{(4)} = -(2/21)\sqrt{2\pi/5}Y_{4,2} - (8/105)\sqrt{\pi}Y_{4,0} - (2/21)\sqrt{2\pi/5}Y_{4,-2}$$
$$\mathcal{A}_{yyyz}^{(4)} = -(i/3)\sqrt{\pi/35}Y_{4,3} - (i/7)\sqrt{\pi/5}Y_{4,1} - (i/7)\sqrt{\pi/5}Y_{4,-1} - (i/3)\sqrt{\pi/35}Y_{4,-3}$$
$$\mathcal{A}_{yyyy}^{(4)} = (1/3)\sqrt{2\pi/35}Y_{4,4} + (2/21)\sqrt{2\pi/5}Y_{4,2} + (2/35)\sqrt{\pi}Y_{4,0} + (2/21)\sqrt{2\pi/5}Y_{4,-2} + (1/3)\sqrt{2\pi/35}Y_{4,-4}$$
$$\mathcal{A}_{xzzz}^{(4)} = -(4/21)\sqrt{\pi/5}Y_{4,1} + (4/21)\sqrt{\pi/5}Y_{4,-1}$$
$$\mathcal{A}_{xyzz}^{(4)} = -(2i/21)\sqrt{2\pi/5}Y_{4,2} + (2i/21)\sqrt{2\pi/5}Y_{4,-2}$$
$$\mathcal{A}_{xyyz}^{(4)} = (1/3)\sqrt{\pi/35}Y_{4,3} + (1/21)\sqrt{\pi/5}Y_{4,1} - (1/21)\sqrt{\pi/5}Y_{4,-1} - (1/3)\sqrt{\pi/35}Y_{4,-3}$$
$$\mathcal{A}_{xyyy}^{(4)} = (i/3)\sqrt{2\pi/35}Y_{4,4} + (i/21)\sqrt{2\pi/5}Y_{4,2} - (i/21)\sqrt{2\pi/5}Y_{4,-2} - (i/3)\sqrt{2\pi/35}Y_{4,-4}$$
$$\mathcal{A}_{xxzz}^{(4)} = (2/21)\sqrt{2\pi/5}Y_{4,2} - (8/105)\sqrt{\pi}Y_{4,0} + (2/21)\sqrt{2\pi/5}Y_{4,-2}$$
$$\mathcal{A}_{xxyz}^{(4)} = (i/3)\sqrt{\pi/35}Y_{4,3} - (i/21)\sqrt{\pi/5}Y_{4,1} - (i/21)\sqrt{\pi/5}Y_{4,-1} + (i/3)\sqrt{\pi/35}Y_{4,-3}$$
$$\mathcal{A}_{xxyy}^{(4)} = -(1/3)\sqrt{2\pi/35}Y_{4,4} + (2/105)\sqrt{\pi}Y_{4,0} - (1/3)\sqrt{2\pi/35}Y_{4,-4}$$
$$\mathcal{A}_{xxxz}^{(4)} = -(1/3)\sqrt{\pi/35}Y_{4,3} + (1/7)\sqrt{\pi/5}Y_{4,1} - (1/7)\sqrt{\pi/5}Y_{4,-1} + (1/3)\sqrt{\pi/35}Y_{4,-3}$$
$$\mathcal{A}_{xxxy}^{(4)} = -(i/3)\sqrt{2\pi/35}Y_{4,4} + (i/21)\sqrt{2\pi/5}Y_{4,2} - (i/21)\sqrt{2\pi/5}Y_{4,-2} + (i/3)\sqrt{2\pi/35}Y_{4,-4}$$
$$\mathcal{A}_{xxxx}^{(4)} = (1/3)\sqrt{2\pi/35}Y_{4,4} - (2/21)\sqrt{2\pi/5}Y_{4,2} + (2/35)\sqrt{\pi}Y_{4,0} - (2/21)\sqrt{2\pi/5}Y_{4,-2} + (1/3)\sqrt{2\pi/35}Y_{4,-4}$$

$X_{\vec{\ell}}(q)$. One could then perform the same operation for mixed pairs. Thus, both X and B could be obtained in a straight-forward manner without ever having introduced a binning in $\cos\theta$ and ϕ.

Although calculating $X_{\vec{\ell}}$ and $B_{\vec{\ell}}$ is straight-forward, finding $C_{\vec{\ell}}$ can be more difficult. Here, we outline the procedure, beginning by expanding $X(\Omega)$, $B(\Omega)$ and $\mathcal{C}(\Omega)$, in terms of unit vector components. One can then require that each term in the expansion is equivalent,

$$\sum_{\vec{\ell}} \gamma(\vec{\ell}) X_{\vec{\ell}} \hat{q}_x^{\ell_x} \hat{q}_y^{\ell_y} \hat{q}_z^{\ell_z} = \sum_{\vec{\ell}} \sum_{\vec{\ell}'=0, \ell_i' \leq \ell_i} \gamma(\vec{\ell}') \gamma(\vec{\ell} - \vec{\ell}') B_{\vec{\ell}'} C_{\vec{\ell}-\vec{\ell}'} \hat{q}_x^{\ell_x} \hat{q}_y^{\ell_y} \hat{q}_z^{\ell_z}. \tag{64}$$

One can uniquely choose $C_{\vec{\ell}}$ to satisfy Eq. (64) for each term, although this solution will not satisfy the tracelessness condition. We will denote this solution as $\bar{C}$.

$$\gamma(\vec{\ell}) X_{\vec{\ell}} = \sum_{\vec{\ell}'=0, \ell_i' \leq \ell_i} \gamma(\vec{\ell}') \gamma(\vec{\ell} - \vec{\ell}') B_{\vec{\ell}'} \bar{C}_{\vec{\ell}-\vec{\ell}'}. \tag{65}$$

The $\ell = 0$ term is straight-forward to extract,

$$\bar{C}_{\ell=0} = \frac{X_{\ell=0}}{B_{\ell=0}}. \tag{66}$$

Given $\bar{C}$ for lower values of ℓ, one can apply Eq. (65) recursively,

$$\bar{C}_{\vec{\ell}} = \frac{\gamma(\vec{\ell}) X_{\vec{\ell}} - \sum_{\vec{\ell}', \ell_i' \leq \ell_i, \ell' < \ell} \gamma(\vec{\ell}') \gamma(\vec{\ell} - \vec{\ell}') B_{\vec{\ell}-\vec{\ell}'} \bar{C}_{\vec{\ell}'}}{\gamma(\vec{\ell}) B_0}. \tag{67}$$

However, since $\hat{q}_x$, $\hat{q}_y$ and $\hat{q}_z$ are not independent, $\hat{q}_x^2 + \hat{q}_y^2 + \hat{q}_z^2 = 1$, there may be other solutions for $C_{\vec{\ell}}$. In particular, we are interested in the solution where the tensor $C_{\vec{\ell}}$ is traceless, i.e., the solution generated by convoluting Cartesian harmonics with the correlation function.

$$C_{\vec{\ell}} = \int \frac{d\Omega}{4\pi} \frac{(2\ell+1)!!}{\ell!} \mathcal{A}_{\vec{\ell}}(\Omega) C(\Omega). \tag{68}$$

To find the unique traceless representation of C, we first find coefficients for the expansion in terms of Cartesian harmonics, $\tilde{C}$.

$$C(\Omega) = \sum_{\vec{\ell}} \gamma(\vec{\ell}) \bar{C}_{\vec{\ell}} \hat{q}_x^{\ell_x} \hat{q}_y^{\ell_y} \hat{q}_z^{\ell_z} = \sum_{\vec{\ell}'} \gamma(\vec{\ell}') \tilde{C}_{\vec{\ell}'} \mathcal{A}_{\vec{\ell}'}(\Omega). \tag{69}$$

Expanding the product of unit-vector components in terms of Cartesian harmonics using Eq. (58), allows one to identify expansion coefficients for $\tilde{C}$,

$$\tilde{C}_{\vec{\ell}} = \sum_{\vec{m}} \bar{C}_{\vec{\ell}+2\vec{m}} \left(\frac{1}{2}\right)^m \frac{(\ell+2m)!}{\ell! m_x! m_y! m_z!} \frac{(2\ell+1)!!}{(2\ell+2m+1)!!} \tag{70}$$

One can now find the coefficients of the expansion of $C(\Omega)$,

$$C_{\vec{\ell}} = \int \frac{d\Omega}{4\pi} \frac{(2\ell+1)!!}{\ell!} A_{\vec{\ell}}(\Omega) C(\Omega) \tag{71}$$

$$= \frac{1}{4\pi} \sum_{\vec{\ell}'} \langle \vec{\ell} | \vec{\ell}' \rangle \frac{(2\ell+1)!!}{\ell!} \gamma(\vec{\ell}') \tilde{C}_{\vec{\ell}'}, \tag{72}$$

where the overlap integrals are given in Eq. (60). If the coefficients $\bar{C}_{\vec{\ell}}$ had satisfied the tracelessness condition, the coefficients $\tilde{C}_{\vec{\ell}}$, $\bar{\mathcal{C}}_{\vec{\ell}}$ and $C_{\vec{\ell}}$ would have been identical.

The sum over ℓ must be cut off at some value $\ell_{\rm max}$. If one had calculated $C(\Omega)$ directly by binning in $\cos\theta$ and ϕ, then convoluting with Cartesian harmonics to find $C_{\vec{\ell}}$, one would have had to invoke a finite bin size. The two methods should provide the same results in the limit of small angular bin sizes and large $\ell_{\rm max}$. When dividing arrays, it should be pointed out that even if X and B are non-zero only for a few low values of $\vec{\ell}$, the solution for C might

have significant contributions for large $\vec{\ell}$. In fact, if $B(\Omega)$ is zero for any direction, there will be no solution. If $B(\Omega)$ approaches zero for some angle, the cutoff $\ell_{\rm max}$ must be large to reproduce the pole-like behavior of $C(\Omega)$.

The second part of this procedure, where a traceless array $C_{\vec{\ell}}$ was found that was equivalent to the array $\bar{C}_{\vec{\ell}}$ represents a method for detracing arbitrary arrays, and could be be used to find the projection operators discussed in the previous subsection. This procedure could also have been used to invert an array. By defining $X_{\vec{\ell}}$ in Eq. (63) to be unity for $\ell = 0$ and zero otherwise, solving for $C_{\vec{\ell}}$ would represent finding the inverse of the array $B_{\vec{\ell}}$.

A similar, but somewhat simpler, procedure can be used to multiply arrays. For instance if one considers the expansion from Eq. (64), where one is given $B_{\vec{\ell}}$ and $C_{\vec{\ell}}$, one could find an array $\bar{X}_{\vec{\ell}}$ that satisfies Eq. (64),

$$\bar{X}_{\vec{\ell}} = \sum_{\vec{\ell}'=0,\ell'_i\leq\ell_i} \frac{\gamma(\vec{\ell}')\gamma(\vec{\ell}-\vec{\ell}')}{\gamma(\vec{\ell})} B_{\vec{\ell}'} C_{\vec{\ell}-\vec{\ell}'}, \tag{73}$$

where in this case $\bar{X}_{\vec{\ell}}$ does not satisfy the tracelessness condition. One can find the equivalent array $X_{\vec{\ell}}$ with the same procedure outlined above to detrace $\bar{C}_{\vec{\ell}}$.

Thus, one can define procedures to multiply, divide and invert arrays without resorting to binning in $\cos\theta$ or ϕ, and without performing matrix inversion operations.

IV. INTERPRETATION OF $\mathcal{S}_{\ell,m}(r)$

The expansion of source functions and correlations functions in spherical harmonics is principally motivated by the simple correspondence between $\mathcal{R}_{\ell,m}(q)$ and $\mathcal{S}_{\ell,m}(r)$ with the same ℓ and m. This reduces the problem of generating the source functions to a series of one-dimensional deconvolutions. The disadvantage of this basis is that the various moments are not so physically transparent. Cartesian harmonics also have the advantage of directly relating projections of the source function and correlation function with the same indices, but are more geometrically transparent. The disadvantage of Cartesian harmonics is that they over-span the space of given angular momentum multiplet, and have complicated orthogonality and normalization properties. Fortunately, as shown in the previous section, it is straight-forward to translate from one basis to the other.

A. Geometric Interpretation of Cartesian Harmonics

The Cartesian moments for $\ell = 1$ would be zero for the source function for identical particles since the distribution of spatial separations must be an even function of $\mathbf{r}$. For non-identical particles the separations can be biased in a given direction. For instance, if protons are emitted earlier than pions, the distributions of relative coordinates, $\mathbf{r}_p - \mathbf{r}_\pi$, will be stronger in the outward direction than in the opposite direction. The three Cartesian moments for $\ell = 1$ source function, $\mathcal{S}_i^{(\ell=1)}$, specify the direction and magnitude of this bias. Thus, the $\ell = 1$ moments address the same issues as the methods proposed by Lednicky [26], where the correlation functions for positive and negative $q_{\rm out}$ were compared. The advantage of Cartesian moments is that more appropriately weight the most relevant relative momentum components, and allow one to determine the direction of the anisotropy, if it is not known from symmetry considerations.

For $\ell = 2$, there are 5 independent projections with spherical harmonics, which can be used to determine the six projections from Cartesian harmonics. The matrix of second power Cartesian Harmonics, $\mathcal{S}_{ij}^{(2)}(r)$, is real, Hermittian and traceless. The matrix can be diagonalized by a rotation, which can be described in terms of Euler angles, $(\phi^{(2)}, \theta^{(2)}, \psi^{(2)})$. If one thinks of the source as having an elliptic anisotropy, this rotation provides a new coordinate system where the three axes represent the major axes of the ellipse. The diagonal elements of $\mathcal{S}^{(2)}$ in the new coordinate system represent the eccentricities of the ellipse.

The Euler angles and the two surviving moments can be generated from the original moments by first diagonalizing $\mathcal{S}_{ij}$ and finding the eigenvalues, $\lambda^{(\alpha)}$, and the eigenvectors, $v_i^{(\alpha)}$.

$$\mathcal{S}_{ij}^{(2)} v_j^{(\alpha)} = \lambda^{(\alpha)} v_i^{(\alpha)}. \tag{74}$$

The normalized eigenvectors provide the basis vectors for the new coordinate system. The Euler angles required to rotate to the new system can be found by comparing the matrix used to rotate to the new basis, U, with the general

expression for rotation by Euler angles, $\theta^{(2)}, \phi^{(2)}, \psi^{(2)}$.

$$U = \begin{pmatrix} v_1^{(1)} & v_2^{(1)} & v_3^{(1)} \\ v_1^{(2)} & v_2^{(2)} & v_3^{(2)} \\ v_1^{(3)} & v_2^{(3)} & v_3^{(3)} \end{pmatrix} \tag{75}$$

$$= \begin{pmatrix} \cos\theta^{(2)}\cos\phi^{(2)}\cos\psi^{(2)} - \sin\phi^{(2)}\sin\psi^{(2)}, & \cos\theta^{(2)}\sin\phi^{(2)}\cos\psi^{(2)} + \cos\phi^{(2)}\sin\psi^{(2)}, & -\sin\theta^{(2)}\cos\psi^{(2)} \\ -\cos\theta^{(2)}\cos\phi^{(2)}\sin\psi^{(2)} - \sin\phi^{(2)}\cos\psi^{(2)}, & -\cos\theta^{(2)}\sin\phi^{(2)}\sin\psi^{(2)} + \cos\phi^{(2)}\cos\psi^{(2)}, & \sin\theta^{(2)}\sin\psi^{(2)} \\ \sin\theta^{(2)}\cos\phi^{(2)}, & \sin\theta^{(2)}\sin\phi^{(2)}, & \cos\theta^{(2)} \end{pmatrix}$$

The new set of unit vectors entail a rotation by ϕ about the z axis, a rotation by θ about the new y axis, and a rotation by ψ around the revised z axis. By permuting the eigenvectors in the definition of U, one can choose which axis is rotated to a particular eigenvector. The Euler angles, like the eigenvectors, are implicitly functions of r. The same techniques described above for re-expressing the information in $\mathcal{S}_{ij}^{(2)}(r)$ can be applied to $\mathcal{R}_{ij}^{(2)}(q)$. If the eigenvectors of v_i are independent of r, the same eigenvectors will diagonalize the corresponding Cartesian tensor, $\mathcal{R}_{ij}^{(2)}(q)$.

For $\ell > 2$, a natural coordinate system is one where one of the axes points along the direction where $\mathcal{S}^{(\ell)}(\Omega) \equiv \mathcal{S}^{(\ell)}_{\alpha_1\cdots\alpha_\ell}\hat{r}_{\alpha_1}\cdots\hat{r}_{\alpha_\ell}$ is maximized. If this direction is defined as the new z axis, $\mathcal{S}_{\ell_x=0,\ell_y=1,\ell_z=\ell-1}$ and $\mathcal{S}_{\ell_x=1,\ell_y=0,\ell_z=\ell-1]}$ are zero. If one also defines the x axis as the direction perpendicular to the z axis where $\mathcal{S}^{(\ell)}(\Omega)$ is minimized, $\mathcal{S}^{(\ell)}_{\ell_x=\ell-1,\ell_y=1,\ell_z=0}$ is also constrained to be zero.

B. Advantages and limitations of Analyzing with Spherical and Cartesian Harmonics

For a given value of the total momentum, correlation functions provide three dimensions of information about the source function. Effectively, there are two competing approaches for extracting the three dimensions of information contained in $\mathcal{R}(\mathbf{q})$. First, one could perform a three-dimensional fit to the correlation function. This requires choosing a parameterization and fitting the various parameters. Given the large number of parameters one might want to use to describe a three-dimensional source, it can be difficult to discern which aspects of the source were well determined by the fit. Decomposing the problem with spherical harmonics has the distinct advantage of reducing the problem to a series of one-dimensional problems. The one-to-one correspondence between the specific angular components of $\mathcal{S}$ and the same moments of $\mathcal{R}$ provides a clear connection between identifiable properties of the measured correlation function and identifiable properties of the source function. Whether one is approaching the analysis as an inversion problem or as a fitting exercise, it is certainly preferable to divide and conquer, i.e., to attack the problems as a series of one-dimensional problems.

Spherical decompositions of correlation functions carry more information than can be expressed with Gaussian source parameters. The nine source functions $\mathcal{S}_{\ell,m}(r)$ for $\ell \leq 2$ uniquely determine the moments $\langle r_i r_j\rangle$ and $\langle r_k\rangle$ for all i, j and k. These nine moments determine all the nine Gaussian source parameters, which are discussed in detail in the next section. By studying moments with $\ell > 2$ one accesses shape information that is inaccessible to Gaussian fits. Gaussian sources can be rotated into a frame where there are no cross terms and the moments obey a factorization constraint,

$$\langle x^{\ell_x} y^{\ell_y} z^{\ell_z}\rangle = \langle x^{\ell_x}\rangle\langle y^{\ell_y}\rangle\langle z^{\ell_z}\rangle. \tag{76}$$

This factorization does not hold in general. For instance, for correlations of two particles with different masses coming from a boost-invariant source, as discussed in Sec. V B, the moment $\langle r_{\rm out} r^2_{\rm long}\rangle \neq \langle r_{\rm out}\rangle\langle r^2_{\rm long}\rangle$. This failure of factorization is due to the "boomerang" shape of the outgoing probability cloud. This shape is due to the fact that the particles from a boost-invariant source that come from the region with z near zero are emitted before the particles with larger values of z. The boomerang shape can be investigate by analyzing Cartesian moments of order $\ell \leq 3$, which through Eq. (59) can yield the moments $\langle xy^2\rangle$ and $\langle xz^2\rangle$, which can then be compared to $\langle x\rangle\langle y^2\rangle$ and $\langle x\rangle\langle z^2\rangle$.

Although it is straightforward to define $\mathcal{R}_{\ell,m}(q)$ as a convolution of the correlation with $Y_{\ell,m}(\Omega_q)$, some caveats should be listed concerning the choice of the range of relative momentum q and the choice of coordinate system. The range of q can be especially touchy given the presence of other sources of correlation. Coulomb kernels fall off slowly, $\sim 1/q^2$, for large q which makes it tempting to exploit the information in the tails of the correlation function. However, as q increases other types of correlation begin to compete with the correlation from final-state interactions. For pp correlations, the strength of the correlation from final-state Coulomb interactions is typically of the order of one percent for q near 100 MeV/c. For $p\pi^+$ correlations, the strength of the correlation for $q = 225$ MeV/c, where

the Δ resonance dominates, is also of the order of one percent. Correlations from elliptic and directed flow can also be of the order of a few percent and tend to peak at values of q near the mean p_t (a few hundred MeV/c). The contribution from such correlations can be largely eliminated by corrections for the reaction plane, but it is probably wise to steer away from trying to exploit final-state-interaction correlations that are much smaller than a half percent. At high energy, jets represent another source of correlation. These are also of the order of one percent for lower p_t particles and the scale of the correlation is also of the order of several hundred MeV/c. Since it is difficult to subtract the contribution from jets, it underscores the importance of staying away from correlations that are below the half percent scale.

Another advantage of moment analyses comes from the fact that the shape information in $S^{(\ell)}(r)$ can depend on r. Several studies have focused on determining the non-Gaussian behavior of the angle-averaged source function, $\mathcal{S}^{(\ell=0)}(r)$. The $\ell > 0$ source functions can be dramatically non-Gaussian. For instance, long-lived sources should have exponential tails in the outwards direction if emission falls off as $e^{-t/\tau}$. This should be especially true for non-explosive, gradually cooling sources, or for particles which come principally from the decay of long-lived heavy resonances. At high-energy the sources should become boost invariant. Boost invariant thermal sources have the form,

$$\frac{dN}{dzdt} \sim \delta(\tau - \tau_0) e^{-E_\perp/T)\sqrt{1+z^2/\tau^2}}, \tag{77}$$

where $\tau = (t^2 + z^2)^{1/2}$. These sources fall off exponentially in the z direction. Since $\mathcal{S}_{\ell_x=0,\ell_y=0,\ell_z=2}$ projection should be especially pronounced at large r.

When analyzing shapes, it should be stressed that for small r,

$$\mathcal{S}^{(\ell)}(r) \sim r^\ell. \tag{78}$$

Furthermore, since the convolution with the kernel has an extra weight of r^2 from phase space, shape analyses will have most sensitivity at larger values of r. This underscores the importance of understanding the large-r behavior of the kernels discussed in the previous section.

V. EXAMPLES

A. Gaussian Sources

Many analyses of correlation functions involve extracting Gaussian source-size parameters. Gaussian parameterizations are popular because they allow the most important spatial information about $\mathcal{S}(\mathbf{r})$ to be expressed in terms of a minimal number of parameters.

For identical particles, the Gaussian functions must obey a reflection symmetry about the point $\mathbf{r} = 0$. The Gaussian source function can then be described in terms of the six parameters composing the symmetric matrix $(1/R^2)$, where the source function is

$$\mathcal{S}(\mathbf{r}) = \frac{[\det(1/R^2)]^{1/2}}{(4\pi)^{3/2}} \exp\left\{-\frac{1}{4}\left(\frac{1}{R^2}\right)_{ij} r_i r_j\right\}, \tag{79}$$

Rather than describing the source function with these six parameters, it is perhaps more physically intuitive to express the source function by first rotating to a coordinate system where $(1/R^2)$ is diagonal. The three Euler angles required for the rotation replace the three cross terms of the matrix. The diagonal elements then represent the dimensions along each of the three principal axes.

For non-identical particles, there is no longer a constraint that $\mathcal{S}(\mathbf{r})$ should be symmetric about $\mathbf{r} = 0$. The offsets can be easily incorporated into the source function,

$$S(\mathbf{r}) = \frac{1}{(4\pi)^{3/2} R_x R_y R_z} \exp\left\{-\frac{(x - X_{\rm off})^2}{4R_x^2} - \frac{(y - Y_{\rm off})^2}{4R_y^2} - \frac{(z - Z_{\rm off})^2}{4R_z^2}\right\} \tag{80}$$

The source function is then described by nine parameters: the three Euler angles that diagonalized $(1/R^2)$, the three dimensions R_x, R_y and R_z, and the three offsets. The offsets are of interest in both intermediate-energy and high-energy collisions [26, 27]. For instance, at low energy one would be interested to know whether neutron emission preceeded proton emission, or whether intermediate-mass fragments were emitted simultaneously with the protons [28]. At high energy, one might look for evidence of strange particles leaving early [29]. Furthermore, simultaneous

emission combined with radial expansion leads to heavier particles being offset further in the outwards direction relative to lighter particles [30].

Source symmetries often allow one to choose coordinate systems where the cross terms vanish and eliminate the need to calculate the Euler angles [1]. For example, for central collisions of identical nuclei, correlations for particles near mid-rapidity are usually analyzed in the "out-long-side" coordinate system. The "out-long" cross term becomes non-zero when one moves away from mid-rapidity or if the collision is not central. The "out-side" cross term is non-zero whenever the collision is not central, and the "long-side" cross term can be non-zero away from mid-rapidty, but only for non-central collisions.

The nine Gaussian parameters described above can be related to the moments of the correlation functions. It is tempting to link the three $\ell = 1$ moments with the off-sets and to link the five $\ell = 2$ moments with the non-spherical shape of the Gaussians. But, such correspondences are not exact. For instance, one can consider a simple spherical form for $\mathcal{S}(\mathbf{r})$ that is offset in the z direction.

$$\begin{aligned} \mathcal{S}(\mathbf{r}) &= \frac{1}{(4\pi)^{3/2}R^3}\exp\left\{-\frac{x^2+y^2+(z-Z_{\rm off})^2}{4R^2}\right\}, \\ \mathcal{S}_{\ell,m}(r) &= \frac{1}{(4\pi)^{3/2}R^3}e^{-(r^2+Z_{\rm off}^2)/(4R^2)}\int\frac{d\Omega}{(4\pi)^{1/2}}Y_{\ell,m}(\Omega)\exp\left\{\frac{Z_{\rm off}z}{2R^2}\right\} \\ &= \frac{i^\ell(2\ell+1)^{1/2}}{(4\pi)^{3/2}R^3}e^{-(r^2+Z_{\rm off}^2)/(4R^2)}j_\ell\left(i\kappa r\right)\delta_{m,0}, \end{aligned} \tag{81}$$

where $\kappa = Z_{\rm off}/(2R^2)$ and the spherical Bessel function comes from making a "plane-wave" expansion of the exponential $e^{\kappa z}$. Thus, Eq. (81) illustrates that an offset results in non-zero moments for all $\ell > 1$ even though the shape of the source is spherically symmetric about the offset point. Since $j_\ell(i\kappa r)$ rises as $(\kappa r)^\ell$ for small r, the higher moments exist mainly at large r.

Despite the apparent simplicity of Gaussian forms, calculating the decomposition of a Gaussian into spherical or Cartesian harmonics is not trivial. Since the argument of the exponential is quadratic in x, y and z, it can be expanded in spherical harmonics using only $\ell \leq 2$. However, expanding the exponential results in harmonics to all orders. To demonstrate how to calculate the result to all orders for an arbitrary Gaussian we first label the argument of the exponential in Eq. (80) as Γ.

$$\begin{aligned} S(\mathbf{r}) &= Ce^{\Gamma}(\mathbf{r}), \\ \Gamma(\mathbf{r}) &= \sum_{\ell,m}\gamma_{\ell,m}(r)Y_{\ell,m}(\theta,\phi). \end{aligned} \tag{82}$$

It is straight-forward to express the expansion coefficients $\gamma_{\ell=0,1,2,m}$ in term of the argument of the exponential in the Gaussian. The exponential can be expanded in powers of Γ which allows it to be expressed recursively,

$$\begin{aligned} e^{\Gamma(\mathbf{r})} &= \sum_{N=0}^{\infty}S_N(\mathbf{r}), \\ S_N(\mathbf{r}) &= S_{N-1}(\mathbf{r})\frac{\Gamma(\mathbf{r})}{N}. \end{aligned} \tag{83}$$

After expressing both S and Γ in terms of spherical harmonics, Clebsch-Gordan algebra can be applied to find a recursive expression for the moments of S.

$$S_{N,\ell,m}(r) = (4\pi)^{1/2}\sum_{\ell-2\leq\ell'\leq\ell+2,\ell,m'}\langle\ell,m|\ell',m-m',\ell,m'\rangle S_{N-1,\ell',m-m'}(r)\gamma_{\ell,m'}(r)/N. \tag{84}$$

One can apply Eq. (84) to iteratively calculate $S(N)$ for increasing values of N. If $R_{\rm min}$ is the smallest dimension of the source, the sum saturates for N much larger than r/R.

An analogous prescription exists for Cartesian harmonics. For Cartesian harmonics, one can express Γ from Eq. (82) in powers of the unit vector with $\ell \leq 2$,

$$\Gamma(\mathbf{r}) = \sum_{\vec{\ell},\ell\leq 2}\beta_{\vec{\ell}}(r)\hat{r}_x^{\ell_x}\hat{r}_y^{\ell_y}\hat{r}_z^{\ell_z}, \tag{85}$$

where the coefficients $\beta_{\vec{\ell}}$ can easily be determined from the form of the argument of the Gaussian. One can then recursively find expressions for S_N,

$$e^{\Gamma(\mathbf{r})} = \sum_N S_N(\mathbf{r}), \tag{86}$$

$$S_{N,\vec{\ell}}(r) = (1/N) \sum_{\vec{m},m\leq 2} S_{N-1,\vec{\ell}-\vec{m}}(r)\beta_{\vec{m}}(r). \tag{87}$$

By inspection of the expression for expanding angular functions, Eq. (8), the angular projections of the source function can be given by summing over the terms,

$$\tilde{S}_{\vec{\ell}}(r) = \sum_N \frac{\ell_x!\ell_y!\ell_z!}{\ell!} S_{N,\vec{\ell}}, \tag{88}$$

Although $\tilde{S}$ can be used to express $S(\mathbf{r})$, the coefficients do not satisfy the tracelessness property, Eq. (37). Finding the equivalent detraced tensor can be accomplished with the methods described in in Sec. III.

To illustrate the ability to measure source shapes we consider a simple cylindrically symmetric Gaussian source that incorporates an offset. We choose parameters: $R_x = R_y = 4$ fm, $R_z = 8$ fm, $Z_{\rm off} = 4$ fm. These parameters describe two sources, one for each species, which are elongated along the z-axis by a factor of two. The center of the a-particle source is displaced by an amount $Z_{\rm off}$ along the z axis relative to the center of the b-particle source. Before performing the angular decompositions, we show correlations as a function of $\cos\theta_q$ for fixed q in Fig. 3 for a variety of particle pairs: pK^+, $p\pi^+$, pp, pn, nn and $p\Lambda$. The angular dependence of the correlation functions in Fig. 3 owe their existence to the anisotropic source functions. One can see that these correlations tend to be of the order of a few percent and that the variation with angle tends to be of the same order as the correlation. Correlations at smaller q tend to be stronger, although there is more phase space at large q. By visual inspection, one can recognize that the dependence on $\cos\theta_q$ has both an even and an odd component. The even component derives from the fact that $R_z \neq R_x$, while the odd component derives from the fact that $Z_{\rm off} \neq 0$.

Once the source functions for a Gaussian source are calculated using the iterative procedure outlined above, correlations can then be calculated by convoluting with the kernels using Eq. (4). After generating the source functions in the basis of spherical harmonics, one can apply the equations in Table II to find the source functions in the basis of Cartesian harmonics. Due to the symmetry from rotating about the z axis, all Cartesian components with an odd-number of the x or y indices will be zero. For $\ell \leq 3$, the only non-vanishing moments are $\mathcal{S}^{(0)}, \mathcal{S}^{(1)}_z, \mathcal{S}^{(2)}_{xx}, \mathcal{S}^{(2)}_{yy}, \mathcal{S}^{(2)}_{zz}, \mathcal{S}^{(3)}_{zzz}, \mathcal{S}^{(3)}_{xxz}$ and $\mathcal{S}^{(3)}_{yyz}$. Furthermore the rotational symmetry enforces that $\mathcal{S}^{(2)}_{xx} = \mathcal{S}^{(2)}_{yy}$ and $\mathcal{S}^{(3)}_{xxz} = \mathcal{S}^{(3)}_{yyz}$. The left panel of Fig. 4 shows pK^+ and $p\pi^+$ correlations decomposed into Cartesian harmonics for $\ell \leq 3$. The moments that are not shown can be easily easily generated from the rotational symmetry or from the traceless property, Eq. (37), i.e., $\mathcal{S}^{(2)}_{xx} = -(1/2)\mathcal{S}^{(2)}_{zz}$ and $\mathcal{S}^{(3)}_{zzz} = -(\mathcal{S}^{(3)}_{xxz} + \mathcal{S}^{(3)}_{yyz})$.

The correlations in Fig. 4 are plotted for $q < 80$ MeV/c. In this range the correlation should be dominated by Coulomb effects. Also shown are the pK^+ correlations one would obtain assuming only classical Coulomb effects. As expected from our discussion of the kernels in Section II, quantum effects damp out the correlations for small q, which makes it more difficult to determine characteristics of the shape. The Coulomb hole in the $p\pi^+$ correlation function is weaker than in the pK^+ case due to the smaller reduced mass. Since the region where quantum effects damp the correlation function is confined to $qR/\hbar$ of order ℓ, or less, shape information can be more difficult to extract in $p\pi^+$ correlations than in pK^+ correlations.

Although difficult, it is certainly tenable to measure correlations of the order of one percent or less. In order to better show these correlations, Fig. 5 displays the same correlations as are shown in Fig. 4, only weighted by q^2. One can see that the correlation becomes smaller for increasing ℓ. Since the behavior is fairly smooth in q for all ℓ, one can analyze the correlations in large momentum bins. Since phase space increases as q^2, it should not be difficult to garner sufficient statistics to analyze these correlations despite the fact that they are at the one percent level. The difficulty should be in subtracting competing correlations such as those from collective flow or from jets.

Nucleon-nucleon correlations are good candidates for correlation analyses due to the large scattering lengths which lead to strong correlation structures on the scale of 20 MeV/c. The right-side panel of Fig. 4 displays correlations for pn, nn, pp, $p\Lambda$ pairs. The Gaussian source parameters are chosen to be the same as were used for the pK^+ and $p\pi^+$ correlations illustrated in the left-side panel of Fig. 4. Compared to the Coulomb-dominated cases shown earlier, these correlations tend to be larger in the rangle 40-80 MeV/c and much larger at lower relative momentum. The odd moments vanish for pp and nn since the source functions for identical particles must be even functions of $\mathbf{r}_a - \mathbf{r}_b$. The odd-$\ell$ correlations are especially important for pn correlations in intermediate-energy heavy ion collisions as they address the issue of whether neutrons are emitted earlier than protons. For high-energy collisions $p\Lambda$ correlations are of interest as they can determine whether hyperons leave earlier than protons.

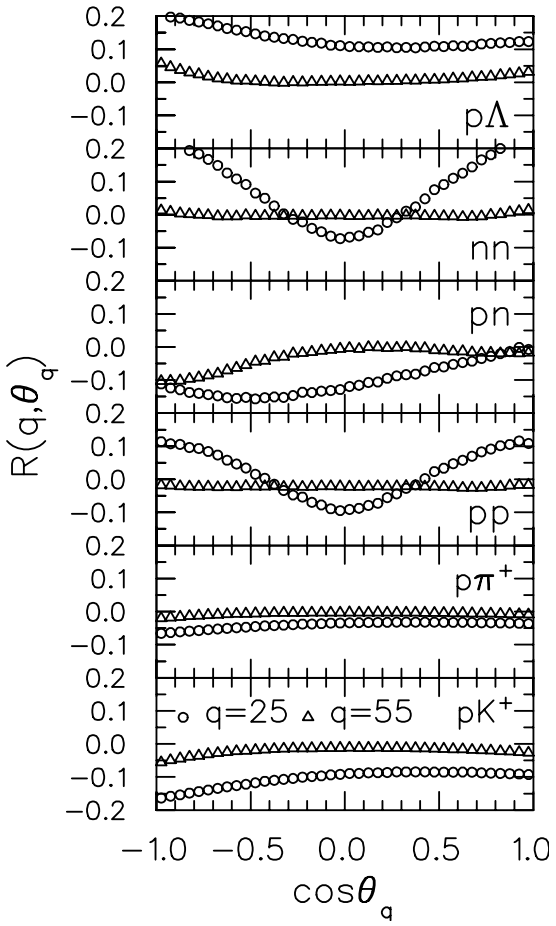

FIG. 3: Correlations for a Gaussian source ($R_x = R_y = 4$ fm, $R_z = 8$ fm, $Z_{\rm off} = 4$ fm) are shown as a function of angle for a variety of particle-pairs at $q = 25$ MeV and at $q = 55$ MeV. The sensitivity to angle is of the same order as the strength of the correlation (~ 1 percent). This shows that extracting shape information usually only requires a modest boost in statistics.

B. Boost-Invariant Blast Wave

Early pion-correlation results from RHIC are remarkably well-fit by blast wave models [30, 31]. These fits suggest nearly instantaneous emission which contradicts a long-lived mixed phase which would have resulted in sequential emission and sources with extended sizes along the "outwards" dimension. Furthermore, a long-lived source would have resulted in longer characteristic sizes for the longitudinal dimension. Given the importance of these measurements, it is important to verify the source-size extractions through other classes of correlations that use kaons or protons.

The minimal blast-wave model we use here has four parameters. Emission is assumed to occur at one proper time $\tau = 10$ fm/c. Collective flow is characterized by linearly increasing transverse rapidities which vary from zero to a maximum $y_{\perp,max} = \tanh^{-1}(v_{\perp,max} = 0.75c)$ at a radius $r_{max} = 13$ fm. The breakup temperature is assumed to be 105 MeV/c. These parameters describe spectra for $p_t < 1$ GeV/c as well as identical pion correlations. For this paper our aim is not to fit data but to use the blast wave as an example to see what behavior one might expect in $\mathcal{R}^{(\ell)}(q)$.

For the purposes of this study, we wish to focus on correlations of non-identical particles since they provide non-zero $\ell = 1$ and $\ell = 3$ moments. Source functions are shown in Fig. 6 for pK and for $p\pi$ source functions. In both cases, the sources are shown for particles moving with a transverse velocity of $0.6c$. The source functions were calculated by randomly generating space-time points for particles with the given velocity consistent with the blast-wave description. After generating several thousand such points, the source function is generated by sampling all such pairs, $\mathbf{r}_a - \mathbf{r}_b$, where $\mathbf{r}_a$ and $\mathbf{r}_b$ are each taken from the list of phase space points for particle types a and b of a given velocity. A few thousand points, which generates a few million pairs, is sufficient to generate a smooth source function, except at very small $|\mathbf{r}_a - \mathbf{r}_b|$.

We choose to associate the beam direction with the z axis and the outward direction with the x axis. Due to the symmetry with respect to the reflections $z \leftrightarrow -z$ and $y \leftrightarrow -y$, there are no Cartesian harmonics with odd numbers

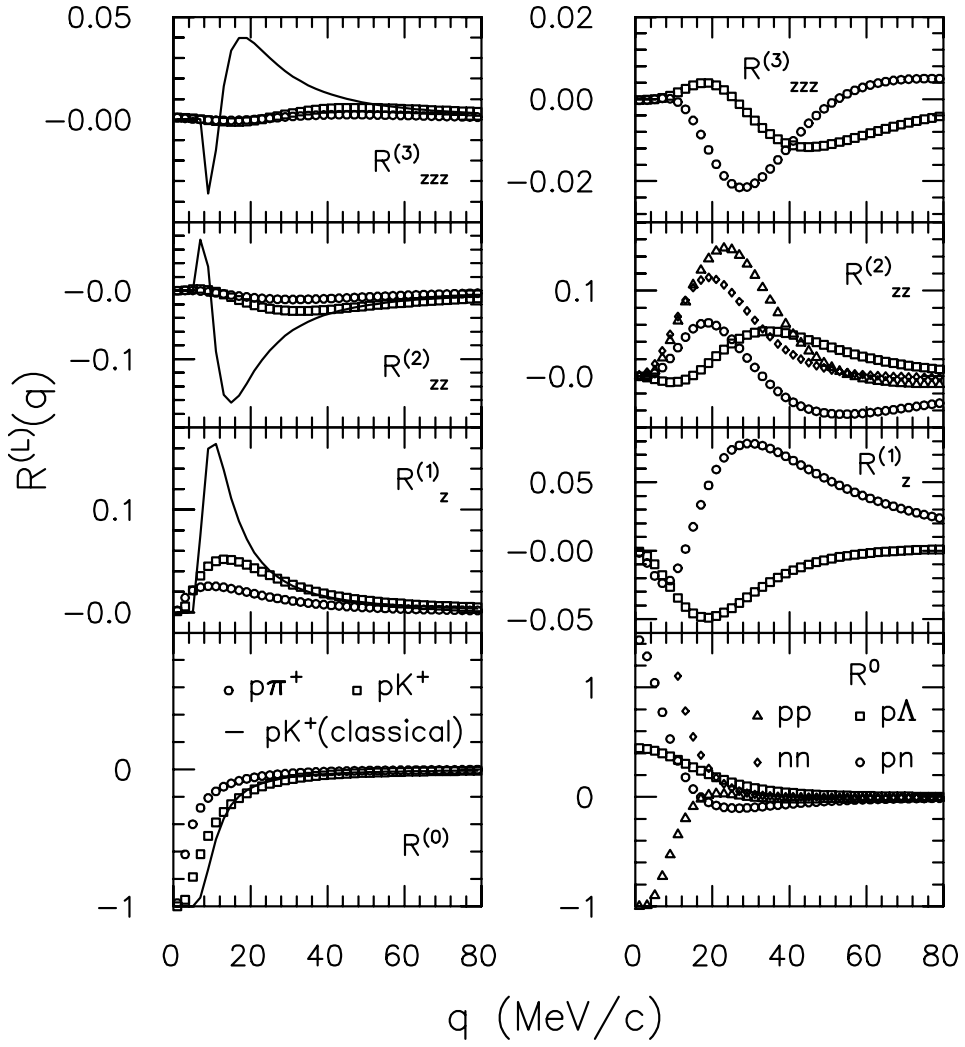

FIG. 4: Correlation functions from a cylindrically symmetric Gaussian source with parameters: $R_x = R_y = 4$ fm, $R_z = 8$ fm and $Z_{\rm off} = 4$ fm. The left panel displays results for pK^+ and $p\pi^+$ pairs. These correlations tend to be dominated by the Coulomb interaction. For pK^+ both quantum and clasical result are displayed which illustrates the degree to which spatial information is damped by quantum effects. Results for various baryon-baryon correlations are displayed in the right panel.

of the z and y indices. Each source function is compared to a Gaussian source whose parameters were chosen to reproduce the moments $\langle x\rangle$, $\langle x^2\rangle$, $\langle y^2\rangle$ and $\langle z^2\rangle$.

Since source functions compare the relative positions of particles moving with the same velocity, the heavier particles tend to be ahead of lighter particles along the outward direction. In an infinite system, i.e., a Hubble expansion, each type of particle would be centered about a point dependent on its own velocity. However, the finite radial size cuts off the outer portion of the emitting region. Since lighter particles have higher thermal velocities, particles of a given velocity are emitted over a greater spatial region and the effect of the cutoff is greater. Thus, for any velocity, pions are more likely to have originated from points closer to the origin than kaons, and kaons are likely to be emitted from points closer to the origin than are protons. Indeed, these offsets have been observed by comparing correlations with $q_{out} > 0$ to those with $q_{out} < 0$ [27, 30]. The $\mathcal{S}_x^{(1)}$ source functions in Fig. 6 illustrate the offset of the centroids of the source functions for the two species. Since the proton and pion have a larger mass difference these moments are noticably larger for the $p\pi$ case than for the pK case. The Gaussian source functions are similar but fail to fit the exponential tails characteristic of the blast waves. Since the Gaussian sources have the same mean $\langle x\rangle$, one would find the same value integrating under the two curves with a weight of r.

The $\ell = 2$ source functions for the blast wave and for the Gaussian again differ principally in the tail. The fact that the Gaussian was chosen to reproduce the Cartesian moments $\langle r_i r_j\rangle$ and $\langle r_i\rangle$ forces the competing curves to integrate to the same values when weighted with r^2. Since an exponential tail is present in the z direction but cut off in the x

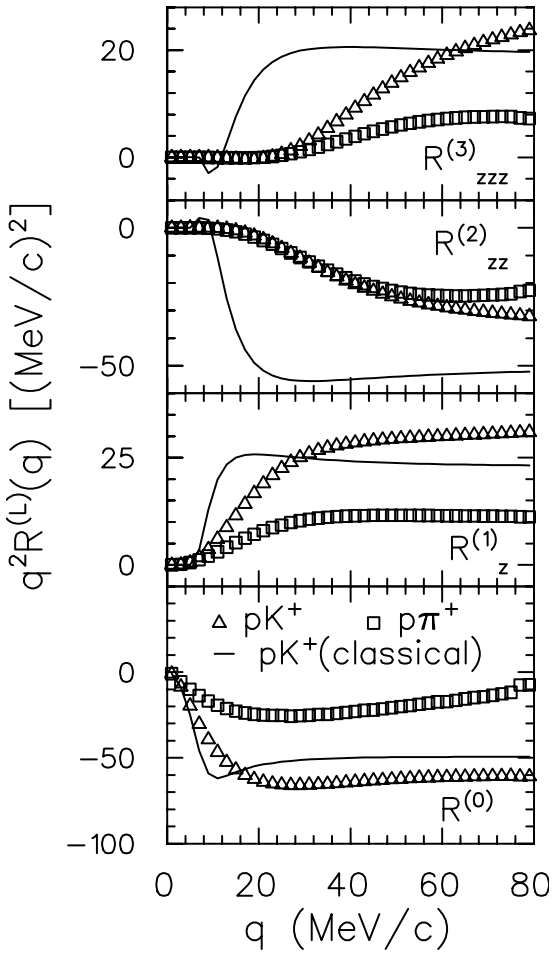

FIG. 5: The same correlations for pK^+ and $p\pi^+$ pairs from Fig. 4 are multiplied by q^2 to better display the strength of the correlation in the tail.

and y directions $\mathcal{S}^{(2)}_{zz}$ is higher for large r in the blast wave calculation than for the Gaussian.

The $\ell = 3$ moments are difficult to interpret since some of the failure of the Gaussian fits stems from the failure to fit the lower moments. The boomerang nature of the source functions should manifest itself in both $\mathcal{S}^{(3)}_{xzz}$ and $\mathcal{S}^{(3)}_{xyy}$. The source function for each species is shaped like a boomerang, so the distribution of relative coordinates is especially complicated.

The Gaussian shapes more closely reproduce the blast wave source functions for the pK case than for the $p\pi$ case. This is likely due to the fact that the blast wave parameterization gives a larger offset for the $p\pi$ than for the pK case due to the larger mass difference. Although the $\ell = 0$ source function has most of its strength below relative separations of 15 fm, the $\ell > 0$ source functions have most of their strength in the 10-25 fm range. Since Coulomb kernels fall as $1/r$, whereas strong-interaction kernels fall as $1/r^2$, Coulomb-induced correlations may be especially well-suited for observing anisotropies since the anisotropies in the source functions are larger at higher r.

Figure 7 displays the correlations calculated by convoluting the kernels with the source functions illustrated in Fig. 6. For both the pK^+ and $p\pi^+$ cases the kernel accounted for both Coulomb and strong interactions. The size of discrepancy between the correlations shown in Fig. 7 for Gaussian and blast-wave sources is similar to the size of the discrepancies seen in Fig. 6 for the corresponding source functions. One can gain a sense of the difficulty in analyzing the shape characteristics by observing the magnitude of the correlations for different ℓ in Fig. 7. For $\ell = 1$, the scale is a few percent, which should be observable with present statistics. For $\ell = 2$, the structures have characteristic structures of one percent. The higher statistics runs of the 2004 RHIC data set should make such analyses quite feasible. Even the 0.1 characteristic sizes of the $\ell = 3$ data sets might be feasible to analyze with these data sets. However, the limiting resolution might be well be determined by systematics rather than by statistics.

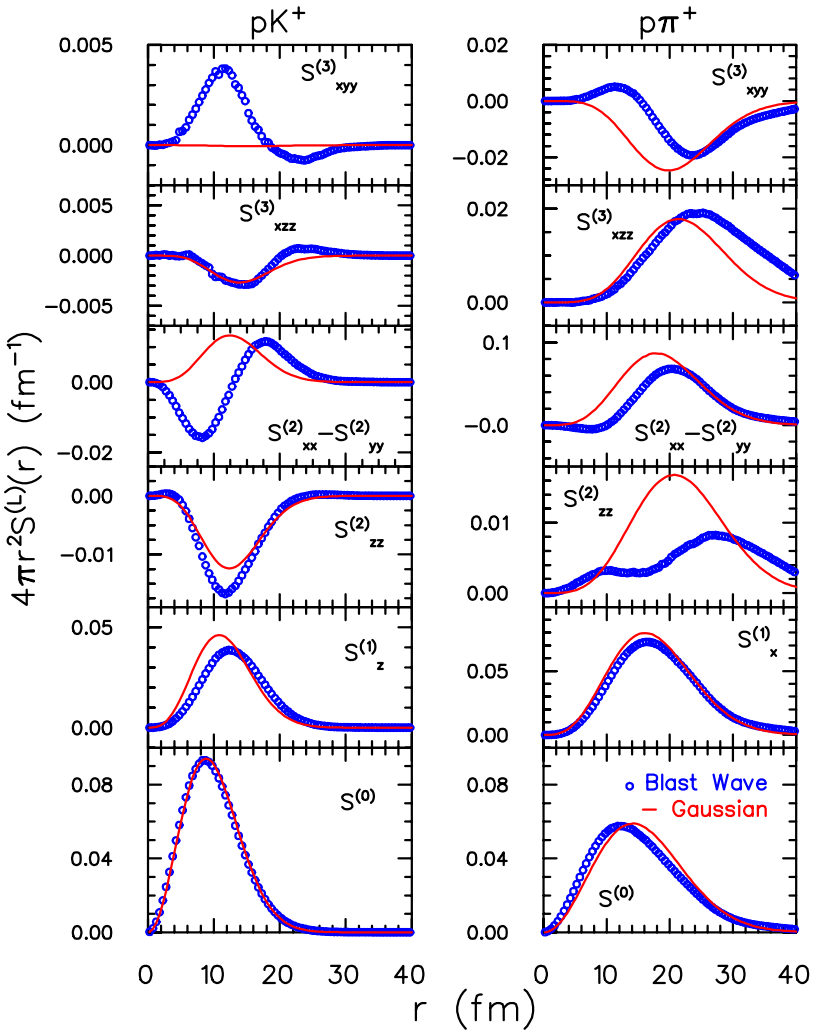

FIG. 6: Source functions are shown pK^+ pairs (left) and for $p\pi^+$ pairs (right) are shown for a thermal blast wave calculation. The results are compared to Gaussian sources with the same Cartesian moments $\langle r_i \rangle$ and $\langle r_i r_j \rangle$. The non-Gaussian behavior is more apparent for the $p\pi$ case because of the larger mass difference.

VI. SUMMARY

Correlation measurements are of crucial importance for deciphering the mire of RHIC data. Without multi-dimensional correlation analyses, there is little hope for understanding the dynamics and the equation of state. To date, such analyses have focused on correlations of identical pions where correlations are largely driven by identical-particle interference. The strong interaction between identical charged pions is small and the Coulomb interaction is independent of shape to a large degree. Since the connection between the source function and the measured correlation function is a Fourier transform, Cartesian coordinates provide a convenient basis for analyzing identical pion correlations.

Correlations that are driven by Coulomb or strong interaction also carry detailed shape information. However, extracting the three-dimensions of coordinate-space information carried by the source function from the three dimensions of information in the measured correlation function is difficult due to the complex six-dimensional form for

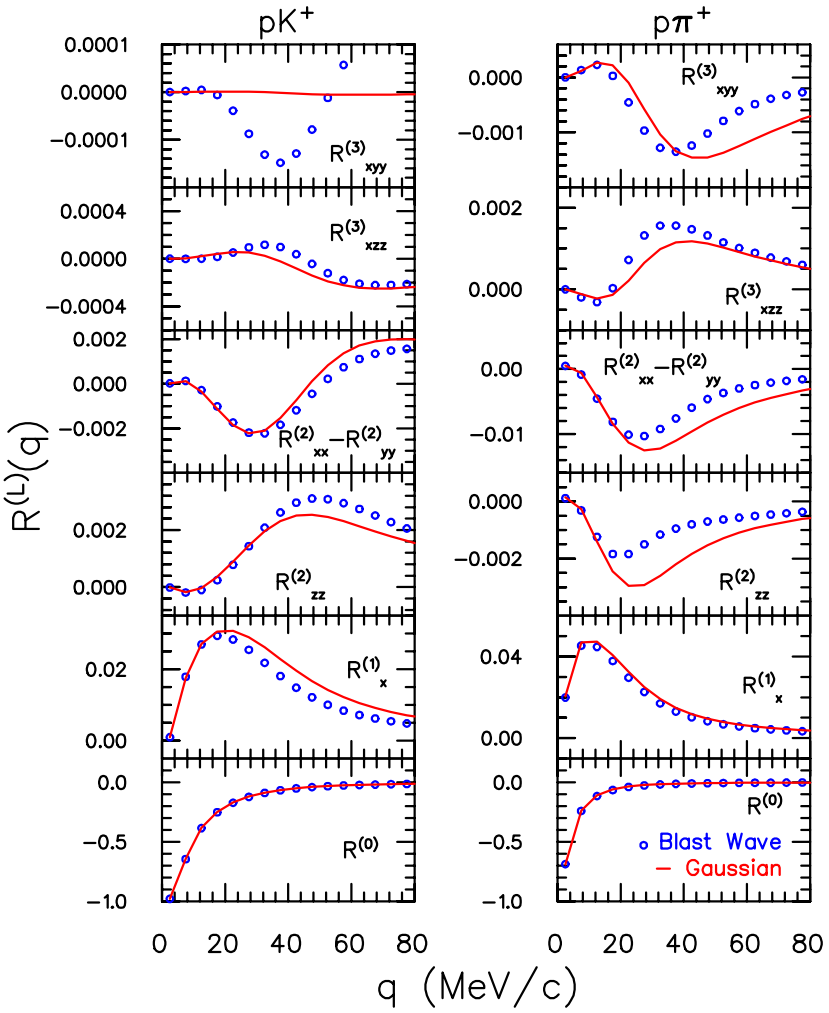

FIG. 7: Correlations for pK^+ pairs and for $p\pi^+$ pairs are shown for the blast wave model described in the text. They are compared to correlations from Gaussian sources that had the same mean offsets and r.m.s. radii. As was true for the source functions in Fig. 6, the difference with Gaussian sources is more pronounced for the $p\pi^+$ case.

the squared wave function. Decomposing the correlation and source functions with spherical or Cartesian harmonics reduces the convolution to a series of one-dimensional problems for each label of the projection. These bases facilitate a more effective interpretation of the data, especially for features of the shape.

The ability to discern information about source shapes from correlation measurements depends on the structure of the kernels, $\mathcal{K}_\ell(q,r)$. In Section II it was shown that identical-particle interference, Coulomb and strong interactions all provide effective kernels. The Coulomb interaction was shown to be provide the greatest resolving for heavier or more highly charged pairs. Strong interactions were shown to be most effective for large cross sections, which tends to happen either at lower relative momenta, or at resonances. Even purely s wave interactions can provide kernels of good resolving power at higher ℓ.

Expansions using spherical harmonics provide a powerful means for storing the angular information in correlation functions, but do not provide as transparent or as intuitive means for understanding the shapes as do a Cartesian basis. Cartesian harmonics have a variety of interesting properties which allow convenient manipulation of angular

information as was shown in Sec. III. The connection between specific aspects of the source geometry and specfic angular moments was emphasized in Sec. IV. It was shown that the spatial offset of the sources for non-identical particles can be examined with the $\ell = 1$ moments and that the shape of the source, e.g., $R_{\rm out}/R_{\rm side}$, or $R_{\rm side}/R_{\rm long}$, can be studied with the $\ell = 2$ moments. Moments for $\ell = 3$ were shown to be sensitive to both the octupole or "boomerang" aspects of the shape.

Section V presented detailed examples. Using Gaussian examples, it was demonstrated that significant shape information is contained in pK^+ or π^+p correlations. Here the strength of the correlation is of the order of one percent or less. Although the upcoming data sets at RHIC will provide statistics that well accommodate the analyses of one percent correlations, the challenge will involve the subtraction of competing correlations, e.g., jets. Strong interactions between a variety of baryons was also shown to provide a good means for discerning shape at small relative momentum. These correlations were of the same order or gretater than the pK^+ correlations which were driven by Coulomb effects. One common feature of all the pairs examined here is that the variation of the correlation with angle is typically of the same strength as the angle-integrated correlation. Hence, if one has sufficient statistics to measure a one-dimensional correlation function, it takes a only a modest enhancement of statistics to find the higher moments. Finally, by calculating correlations for a boost-invariant blast wave model, it was shown that non-Gaussian features of the source function could be brought out in these analyses. Even the slight boomerang shape to the source was manifest in the correlation functions for $\ell = 3$.

In conclusion, a treasure trove of information lies largely ignored in the huge volumes of data from high-energy collisions. This information can address what is the perhaps the greatest surprise of the first several years of RHIC, the inferred source sizes and shapes from identical-pion correlations. The main difficulty with this new class of correlation analyses is the fact that they tend to be quantitatively small, of the order of one percent. This will require a careful analysis of competing correlations from jets and collective flow, but we believe that the objectives will indeed prove feasible.

Acknowledgments

The authors acknowledge insightful discussions with Richard Lednicky, Support was provided by the U.S. National Science Foundation, Grant No. PHY-02-45009, and by the U.S. Department of Energy, Grant No. DE-FG02-03ER41259.

[1] U. A. Wiedemann and U. W. Heinz, Phys. Rept. **319**, 145 (1999), nucl-th/9901094.
[2] U. W. Heinz and B. V. Jacak, Ann. Rev. Nucl. Part. Sci. **49**, 529 (1999), nucl-th/9902020.
[3] W. Bauer, C. K. Gelbke, and S. Pratt, Ann. Rev. Nucl. Part. Sci. **42**, 77 (1992).
[4] B. Tomasik and U. A. Wiedemann (2002), hep-ph/0210250.
[5] C. Adler et al. (STAR), Phys. Rev. Lett. **87**, 082301 (2001).
[6] K. Adcox et al. (PHENIX), Phys. Rev. Lett. **88**, 192302 (2002).
[7] M. Baker et al. (PHOBOS), nucl-ex/0212009.
[8] M. Gyulassy and D. Rischke, Nucl. Phys. A **608**, 479 (1996).
[9] D. Teaney, J. Lauret, and E. Shuryak, nucl-th/0110037.
[10] S. Soff, S. Bass, and A. Dumitru, Phys. Rev. Lett. **86**, 3981 (2001).
[11] P. F. Kolb and U. Heinz (2003), nucl-th/0305084.
[12] D. Anchishkin, U. W. Heinz, and P. Renk, Phys. Rev. **C57**, 1428 (1998), nucl-th/9710051.
[13] S. Pratt, Phys. Rev. **D33**, 1314 (1986).
[14] G. F. Bertsch, Nucl. Phys. **A498**, 173c (1989).
[15] T. Csorgo, J. Zimanyi, J. Bondorf, H. Heiselberg, and S. Pratt, Phys. Lett. **B241**, 301 (1990).
[16] G. Verde et al., Phys. Rev. **C67**, 034606 (2003), nucl-ex/0301013.
[17] G. Verde et al., Phys. Rev. **C65**, 054609 (2002), nucl-ex/0112004.
[18] S. Y. Panitkin et al. (E895), Phys. Rev. Lett. **87**, 112304 (2001), nucl-ex/0103011.
[19] D. A. Brown and P. Danielewicz, Phys. Rev. **C64**, 014902 (2001), nucl-th/0010108.
[20] D. A. Brown, F. Wang, and P. Danielewicz, Phys. Lett. **B470**, 33 (1999), nucl-th/9908033.
[21] D. A. Brown and P. Danielewicz, Phys. Lett. **B398**, 252 (1997), nucl-th/9701010.
[22] S. Pratt and S. Petriconi, Phys. Rev. **C68**, 054901 (2003), nucl-th/0305018.
[23] Y. Kim, R. de Souza, C. Gelbke, W. Gong, and S. Pratt, Phys. Rev. C **45**, 387 (1992).
[24] J. Applequist, Theor. Chem. Acc **107**, 103 (2002).
[25] P. Danielewicz and S. Pratt, Phys. Lett. **B618**, 60 (2005), nucl-th/0501003.
[26] R. Lednicky, V. L. B. Erazmus, and D. Nouais, Phys. Lett. B **373**, 20 (1996).

[27] S. Voloshin, R. Lednicky, and S. Panitkin, Phys. Rev. Lett. **79**, 4766 (1997).
[28] C. J. Gelderloos et al., **75**, 3082 (1995).
[29] F. Wang and S. Pratt, Phys. Rev. Lett. **83**, 3138 (1999), nucl-th/9907019.
[30] F. Retiere and M. A. Lisa, Phys. Rev. **C70**, 044907 (2004), nucl-th/0312024.
[31] B. Tomasik (2004), nucl-th/0409074.